NATIONAL ADVISORY COMMITTEE FOR AERONAUTICS

TECHNICAL NOTE 4239

EXPERIMENTAL INVESTIGATION OF THE DRAG OF FLAT PLATES AND CYLINDERS IN THE SLIPSTREAM OF A HOVERING ROTOR

By John W. McKee and Rodger L. Naeseth

Langley Aeronautical Laboratory
Langley Field, Va.

Washington
April 1958

NATIONAL ADVISORY COMMITTEE FOR AERONAUTICS

TECHNICAL NOTE 4239

EXPERIMENTAL INVESTIGATION OF THE DRAG OF FLAT PLATES AND CYLINDERS IN THE SLIPSTREAM OF A HOVERING ROTOR

By John W. McKee and Rodger L. Naeseth

SUMMARY

An experimental study has been made of the drag of flat plates and cylinders in the slipstream of a hovering rotor. The slipstream was generated by a 6-foot-diameter two-blade rotor with constant-chord untwisted blades. The rotor, drive mechanism, and models were set up outdoors in an area surrounded by walls to minimize wind effects, the slipstream being directed upward to provide an unobstructed model test area and to simulate hovering away from the effect of the ground. Models as large as one with an area equal to 0.212 rotor disk area and a span equal to the rotor diameter were tested in a range of distances from the rotor of 0.10 to 1.33 rotor radii.

The dynamic-pressure profile of the slipstream for stations close to the rotor was characterized by very low or slightly negative values in the center, a rise to a peak near the edge of the slipstream, and a rapid decrease to small negative values farther from the center. Random fluctuations in the slipstream attributed to the effects of wind and proximity of walls made it difficult to obtain precise drag data, even though the values were obtained by averaging recorded data of 1- to 2-minute duration. The drag of constant-chord models spanning the rotor disk was relatively unaffected by distance from the plane of the rotor. From this result it seems that the drag for locations closer than one-quarter rotor radius (at which point the slipstream was effectively fully contracted) is dependent on total energy in the slipstream rather than on dynamic pressure. At distances greater than one-quarter rotor radius, the model drag was found to be determined mainly by the summation of the product of incremental area and dynamic pressure, with unexplained higher drag effects shown for wider chord models and for models spanning the rotor disk. An attempt to compare model drag coefficients with values obtained from wind-tunnel tests led to rather inconclusive results, particularly for the cylinder data which are complexly sensitive to Reynolds number, stream turbulence, and surface finish.

INTRODUCTION

The drag of surfaces and bodies located in the slipstream of a rotor of a hovering helicopter or other rotary-wing aircraft can result in a serious decrease in net thrust. The need for experimental drag results and methods for estimating the loss in thrust has become acute in the design of vertically rising airplanes. The use of drag coefficients obtained from wind-tunnel tests to calculate thrust loss raises questions as to the effect of slipstream turbulence and velocity gradients, both axial and radial, particularly for cases where Reynolds number is known to have a large effect.

Previous investigations (refs. 1 and 2) indicated that the ratio of the drag on a plate spanning the slipstream to the rotor thrust was approximately 0.7 of the fraction of blocked disk area. In reference 2 the drag of a flat plate computed by a strip-analysis method agreed well with experimental results for locations 0.20 to 0.64 rotor radius beneath the plane of zero flapping. It is also conceivable that the presence of a large object in the slipstream could affect the gross thrust or torque of the rotor; however, in reference 2 no change in rotor power at constant thrust due to the presence of the plate was observed.

The present investigation was undertaken to provide an extension of the information presented in references 1 and 2 for a basis of comparison of measured and estimated drag. The drag of flat plates and cylinders and slipstream dynamic-pressure surveys were obtained for a range of distances from the plane of zero flapping of a 6-foot-diameter rotor.

SYMBOLS

D	drag of models, lb; also diameter of strip, in.
q	dynamic pressure, lb/sq ft
ρ	mass density of air, slugs/cu ft
R	rotor radius, ft
S	model area, sq ft
Ω	rotor angular velocity, radians/sec
r	radial distance of instrument or center of model from center of rotor, ft

T	rotor thrust, lb
z	distance from rotor plane of zero flapping to instrument, flat plate, or center line of cylinder, ft
C_Q	torque coefficient, $\text{Torque}/\pi R^2 \rho (\Omega R)^2 R$
ΣqS	summation of product of local dynamic pressure and model area

APPARATUS AND TEST PROCEDURE

An apparatus consisting mainly of a rotor, a rotor-drive mechanism with a 3-horsepower electric motor mounted on a platform scale, and a track along which the platform scale could be moved (fig. 1) was set up in a location chosen for shelter from the wind. The test area (fig. 2) was 17 by 31 feet and was located between a building and a wind tunnel with a temporary wall 19 feet high built on the one open side. The lowest wall enclosing the area was the 19-foot-high temporary wall.

The rotor was 1.8 rotor diameters (11 feet) above the ground and the slipstream was directed upward to provide a model test area unobstructed by the rotor-drive shaft and a slipstream not terminated by a ground plane.

Slipstream dynamic-pressure pickups and models were held above the rotor by an overhead boom hinged to one enclosure wall. An elevated work platform was built onto this wall in a convenient location for making model changes. Traverses of the slipstream were obtained with the position of the support boom fixed by drawing the platform scale and rotor apparatus along the track. Two positions of the rotor disk with respect to the test area are shown in figure 2 as station zero ($r/R = 0$), one for dynamic-pressure surveys and small models and one for 72-inch models. This situation arose from the desire to survey the slipstream from edge to edge as well as to have a range of model positions from the center of the slipstream to outside the slipstream without moving the overhead support.

Rotor

The 6-foot-diameter rotor (fig. 3) had two blades with no twist, was free to cone, and had zero hinge offset and no lag hinges. The blades had NACA 0012 airfoil sections, a solidity of 0.071, and a

constant chord of 0.33 foot from 0.25 radius to the blade tip. The blades were heavy and rigid compared with normal helicopter blades and were ballasted to put the center of gravity of the blade sections on the quarter-chord line.

Models

A sketch of the models tested including the location of the drag balances is given in figure 4. The two rectangular plates were 72 inches long and had 12- and 6-inch chords; the two square plates had 12- and 6-inch edges; and the two cylinders were 72 inches long and 12 and 6 inches in diameter. The areas of the rectangular flat plates and of projections of the cylinders were 0.212 and 0.106 of the rotor-disk area. Each model was mounted with its center of area coinciding with one of the two locations in the test area (fig. 2) marked as station zero ($r/R = 0$) and, unless otherwise noted, the azimuth position of the rectangular plates and cylinders was such that their long dimensions were in the direction of the track which the rotor apparatus traversed.

The rectangular flat plates were made of balsa wood and the square ones were made of 1/8-inch aluminum. The cylinders were made of 1/64-inch aluminum carefully rolled to give a smooth surface. The only lengthwise seam of the cylinder was on the downstream side; the ends were closed; and no attempt was made to polish the surface.

For some tests a round strip, with 0.130-inch diameter, was taped to each side of the 12-inch cylinder to simulate a fuselage discontinuity. (See fig. 5.) The tests were made with the strips at the center line or maximum width and 2 inches above or below this point. Tests were also made with the same strips, with 0.063-inch-diameter strips, and with strips of 0.007-inch by 0.5-inch tape on the center-line position of the 6-inch cylinder.

A model of the upper 0.64 of the Langley helicopter tower (fig. 6) and of the large-span flat plate which was tested in reference 2 was constructed to use in obtaining data for comparison with the results of the reference paper. The plate was tested with $z/R = 0.104$ and 0.55. With the model tower in place, the center of the plate was cut out to provide clearance with the tower.

Instrumentation

The rotor-drive motor was held in the apparatus by bearings at both ends of the motor shaft; thus, the motor case was free to rotate. An arm from the motor case was linked to an electric strain gage which

restrained the case from turning and measured the drive torque. A tare run made with no rotor installed showed that the torque contributed by bearing friction had a negligible value. Rotor thrust was obtained from an electric load cell linked to the weight beam of the platform scales. (See fig. 7.) An oil-filled dashpot was connected to the scale beam to damp vibrations and the load cell was coupled through a spring-loaded link for protection against large overloads.

The drag of the models was measured by one-component balances. Two balances of 6-pound maximum load and one balance of 2-pound maximum load were used. One of the 6-pound balances is shown in figure 8. The balance consisted of a square case made from two pieces of 2- by 2-inch angle and two flexible diaphragms which supported a rod but allowed freedom for axial motion which was restrained by an electric load cell.

A small probe (fig. 9) with a total-pressure and a static-pressure tube connected to a 0.05-pound-per-square-inch electrical pressure cell was used for surveys of dynamic pressure. In addition, surveys were made by using an instrument that determined an effective dynamic pressure by measuring the force on a 0.71-inch-diameter disk. The disk (fig. 10) was supported on an 8-inch shielded lever attached to a strain gage and damped by a small oil-filled dashpot. Both devices used for slipstream surveys were found in calibrations to have a variation in reading of less than 1 percent for angles of attack up to 20°.

The readings from all measuring devices were recorded on chart potentiometers which could not record high-frequency fluctuations but would electrically average fluctuations whose frequency was greater than about 1 per second.

Test Procedure

The survey probes or models mounted on drag balances were set at a height in the range of 0.10 to 1.33 rotor radii above the rotor. The rotor was brought up to speed, and torque, thrust, and dynamic pressure or model drag were recorded for every 2 inches of traverse of the rotor apparatus along the track for the survey probes and at least every 4 inches of traverse for the models.

All tests were run at a rotor speed of 1,167 ± 3 revolutions per minute and a blade pitch angle of 11°. The resulting coning angle was approximately 2°, the tip speed was 367 feet per second, and average torque coefficient C_Q and disk loading (thrust over disk area) were 0.00052 and 1.93 pounds per square foot.

A rotor at zero forward speed may generate a symmetrical slipstream with no random fluctuations under the best of conditions. It is known that a slipstream generated in an enclosed space, even if the space is relatively large, is subject to fluctuations excited by the random recirculation pattern. On the other hand, slipstream distortions are likely to be present in an open outdoor location because periods of true calm are rare in most locations. The magnitude of the effect of wind on slipstream flow is discussed in reference 3. Because of the large number of data points to be taken and the short and not too predictable periods of calm air that could be expected, it was hoped that the air-flow conditions in the sheltered test area would be reasonably steady. Although tests were run during periods of low wind velocity, some disadvantageous effects attributed to the wind, the proximity of walls, and the test procedure of moving the rotor location in the test area were evident in the slipstream characteristics. The time history of the readings with a probe or model in a region of high gradient showed especially large and random variations. It was consistently noted that the slipstream was not centered with respect to the rotor. Rotor thrust and torque were much less subject to variations. It was found necessary to obtain data points for the dynamic-pressure surveys and model drag by averaging chart recordings of 1- to 2-minute duration.

The dynamic-pressure traverses were repeated several times and the data that are presented were selected as the set that showed the greatest symmetry and the most reasonable and consistent trend of change of contour shape with distance from the rotor. In general, only one set of drag data was obtained for each model but in a few instances repeat runs were made and the run that appeared to be most representative was selected for presentation.

RESULTS AND DISCUSSION

Presentation of Data

The results of surveys of the slipstream with the pitot-static probe and with the disk are presented in figure 11. Properties of the slipstream are given in figure 12. The variation in drag of the 6- by 6-inch and 12- by 12-inch plates in pounds per square foot with position is given in figure 13. The data for the other flat plates and the cylinders are given in figures 14 to 17 as the ratio of model drag to rotor thrust. Individual balance readings for models supported by two balances (balances A and B as shown in fig. 2) are given in table I. Some of the data are compared on the basis of percent of blocked disk area in figure 18 and are converted to drag-coefficient form in figure 19.

No definite effect of the presence of models on rotor thrust or torque could be determined from the test data. Results of a special effort to determine whether the largest flat plate when centered over the rotor had a measurable influence seemed to indicate a small increase in measured rotor thrust with no change in power, but even here the results were questionable and are not presented. An average value of rotor thrust of 54.7 pounds was used in the presentation of the data, and, for the configuration proportions of this report, the net thrust can be assumed to be the resultant of the rotor alone minus the drag of the models. The investigations of references 1 and 2 also indicate that no measurable influence of the flat plates on the rotor characteristics could be found.

Rotor Slipstream

The slipstream generated by the untapered, untwisted blades with root cut off at 0.25R was far from uniform, as shown in figure 11. The dynamic pressure for stations close to the rotor is characterized by very low or slightly negative values in the center, a rise to a peak near the edge of the slipstream, and a rapid decrease to small negative values farther from the center. At greater distances from the rotor the dynamic pressure in the center region increases to about half of the peak values near the edge. The slipstream is not centered with respect to the rotor center line (as discussed in "Test Procedure") and the slipstream edge does not vary appreciably with distance from the rotor. Both the total-pressure—static-pressure probe and the 0.71-inch-diameter disk indicated some negative values but the negative points are not shown for the former as it was not calibrated for reverse flow.

The readings obtained from the disk instrument could result from dynamic pressure plus an effect of the average of the pressure pulses that were shown in reference 2 to be very strong close to the rotor. Pressure pulses should have no effect on a pitot-static probe. At the closest station ($z/R = 0.104$), the disk values do seem to be somewhat greater than the pitot-static values. At greater distances from the rotor, the repeatability of the surveys is not exact enough to justify any conclusions. Perfect agreement at distances where pressure pulses are not significant would indicate that the drag coefficient of the disk was the same in the turbulent air of the slipstream as it was in the calibration in the relatively smooth flow in a wind tunnel. Reference 4 indicates that turbulence could cause some increase in the drag coefficient.

The positive pitot-static values of the dynamic pressure were used to determine some of the properties of the slipstream as a function of

distance from the rotor. Integrations were made about an apparent slipstream center to obtain momentum thrust $\left(2\pi \int_{-R}^{R} qr\ dr\right)$, mass flow $\left(\pi\sqrt{2\rho} \int_{-R}^{R} \sqrt{q}\ r\ dr\right)$, average velocity $\left(\frac{\text{Momentum thrust}}{\text{Mass flow}}\right)$, and slipstream power $\left(\pi\sqrt{\frac{2}{\rho}} \int_{-R}^{R} q^{3/2} r\ dr\right)$. These slipstream properties (fig. 12) seem to indicate that the slipstream reaches its maximum contraction by $z/R = 0.25$, followed by a gradual dissipation of energy or mixing process.

The drag loading in pounds per square foot of the square plates is plotted in figure 13 with the q (pitot-static values) from figure 11. The plate drag curves generally resemble the q-curves and show the same off-center tendency. The plate drag loadings show a smoothing or averaging effect compared with the q-distributions, this effect being greater for the larger plate. There is an especially pronounced filling-in effect for the closest station ($z/R = 0.104$) which may be taken to indicate that the pressure pulses have a larger drag effect on these plates than was true for the small disk.

An unsuccessful attempt was made, by computing D/qS, to show more exactly the extent to which the drag of the square plates was not uniquely determined by dynamic pressure obtained from the pitot-static surveys. The variation of drag coefficient with location in the slipstream was very erratic, probably because slipstream variations of dynamic pressure across the plate could not be accurately accounted for and because the variations in dynamic pressure during a run and between runs were too great to obtain precise data. The square-plate drag is presented later in drag-coefficient form for a series of plates covering the same area as the rectangular plates.

Drag-to-Thrust Ratio

The ratio of vertical drag to average rotor thrust is presented in figures 14 and 15 for the rectangular flat plates and in figures 16 and 17 for the cylinders. The data are plotted against fraction-of-rotor-radius displacement of the center of the model from the center of the rotor. The relative positions of the rotor disk and model are shown at the top of the figures.

These figures show similar trends of D/T with model position. Reference to the slipstream surveys of figure 11 is an aid to visualizing

the manner in which the change of drag with model position is dependent upon the part of the slipstream that is becoming unblocked as the model moves to the right. For locations close to the rotor (small z/R), there is a decrease in drag after the model has been moved far enough from $r/R = 0$ (centered in slipstream) that the left end is leaving the high-dynamic-pressure area at the left edge of the slipstream. There is very little change in drag as the end of the model is crossing the center hole in the slipstream and a rapid decrease as the model completely leaves the slipstream. A more linear variation would be expected for blades with taper or twist. As the distance from the rotor z/R is increased, the curves become more linear, as would be expected from consideration of the dynamic-pressure surveys. However, the result that the drag obtained with the models fully immersed in the slipstream was generally considerably more than double the drag obtained with the models half immersed is not readily explained. Additional tests would be required to determine the relative importance of the effect of slipstream contour (presence of hole in the middle, for instance) and aspect-ratio effect of plates with lengths less than, equal to, or greater than the slipstream diameter.

Surface discontinuities in the form of rounded strips running the length of the cylinders (figs. 16(b) and 17(b)) are shown to increase the drag, the greatest effect being shown for strips on the center line. A small discontinuity, 0.007 inch high, had a negligible effect.

Ratio of Percent Thrust Loss to Percent Blocked Area

The data for models spanning the rotor disk have been reduced to the ratio of the percent thrust loss due to model drag over the percent of blocked disk area and are presented in figure 18. This factor has been proposed in references 1 and 2 as a simple relation to estimate the thrust loss. Some caution should be used in making comparisons on this basis, since blocking the slipstream rather than blocking rotor disk area causes thrust loss.

The curves of figure 18 seem impossible to explain in detail but, in general, greater model width results in a higher thrust-loss factor and an increase in z/R does not reduce the thrust loss. The difference shown in the results for two azimuth positions of the 12- by 72-inch plate is further evidence that slipstream distortion was present. When it was found that the drag of the 6- by 72-inch and 12- by 72-inch plates did not show a decrease with distance from the rotor as had been found for a flat plate tested on the Langley helicopter tower (ref. 2), the model simulating that of reference 2 was tested alone and in the presence of a body simulating the upper 0.64 of the tower. The presence of a simulated tower is shown to have an effect and to bring the results into closer agreement with the data of reference 2.

Drag Coefficients

Drag coefficients obtained for rectangular plates and cylinders spanning the slipstream or half the slipstream and for the summation of a series of individual square plates covering the same area as the rectangular plates spanning the slipstream are summarized in figure 19. The coefficients were obtained by dividing the drag of the models by a value of qS obtained by integrating the q (pitot-static) profiles of figure 11. The drag for the rectangular plates was the average of values obtained for several azimuth positions of the plates with respect to the rotor apparatus and test area. The q was assumed to be constant over the 6-inch and 12-inch width of the models.

The high values of drag coefficients shown for low values of z/R (models close to rotor) are not the result of high drag but rather of low dynamic pressure before the slipstream is fully contracted. It is another indication that part of the drag results from the effect of pressure pulses discussed in reference 2. It is of interest to compare the drag coefficients with those obtained from wind-tunnel tests. The value for a flat plate taken from reference 5 is 2.00 for an infinite aspect ratio but values for other aspect ratios are much lower - 1.29 for an aspect ratio of 12, 1.20 for an aspect ratio of 6, and 1.16 for an aspect ratio of 1. The effective aspect ratios of the models are open to question. The model results (the high values for low values of z/R being neglected) group around a drag coefficient of about 1.45, except for the plates spanning the rotor disk which have higher values (as high as 2.0 for $z/R = 0.25$). Comparing cylinder drag coefficients with wind-tunnel values introduces other complicating factors. Cylinders have a critical Reynolds number dependent upon surface finish and stream turbulence (refs. 6 and 7) which, when exceeded, can result in a drag coefficient that is one-third the subcritical value. The highest Reynolds number during the tests (obtained with the 12-inch cylinder) just about equaled the critical value for smooth cylinders in nonturbulent flow. Reference 5 gives subcritical values of 0.79 and 0.85 for length-diameter ratios of 6 and 12, and 1.2 for infinite aspect ratio. These values are about two-thirds the flat-plate values. However, the test cylinder drag coefficients are about one-third the flat-plate values. Evidently even the 6-inch cylinder was effectively subject to a supercritical Reynolds number.

CONCLUDING REMARKS

An experimental study has been made of the drag of flat plates and cylinders in the slipstream of a hovering rotor. The slipstream was generated by a 6-foot-diameter 2-blade rotor with constant-chord untwisted

blades. Tests were made in a sheltered outdoor location. The dynamic-pressure profile of the slipstream for stations close to the rotor was characterized by very low or slightly negative values in the center, a rise to a peak near the edge of the slipstream, and a rapid decrease to small negative values farther from the center. Random fluctuations in the slipstream attributed to the effects of wind and the proximity of walls made it difficult to obtain precise drag data, even though the values were obtained by averaging recorded data of 1- to 2-minute duration. The drag of constant-chord models spanning the rotor disk was relatively unaffected by distance from the plane of the rotor. From this result it appears that the drag for locations closer than one-quarter rotor radius (at which point the slipstream was effectively fully contracted) is dependent on total energy in the slipstream rather than on the dynamic pressure. At distances greater than one-quarter rotor radius, the model drag was found to be determined mainly by the summation of the product of incremental area and dynamic pressure, the higher drag effects shown for wider chord models and for models spanning the rotor disk being unexplained. An attempt to compare model drag coefficients with values obtained from wind-tunnel tests led to rather inconclusive results, particularly for the cylinder data which are complexly sensitive to Reynolds number, stream turbulence, and surface finish.

Langley Aeronautical Laboratory,
National Advisory Committee for Aeronautics,
Langley Field, Va., December 17, 1957.

REFERENCES

1. Fail, R. A., and Eyre, R. C. W.: Loss of Static Thrust Due to a Fixed Surface Under a Helicopter Rotor. Tech. Note No. Aero. 2008, British R.A.E., July 1949.

2. Makofski, Robert A., and Menkick, George F.: Investigation of Vertical Drag and Periodic Airloads Acting on Flat Panels in a Rotor Slipstream. NACA TN 3900, 1956.

3. Gessow, Alfred: Review of Information on Induced Flow of a Lifting Rotor. NACA TN 3238, 1954.

4. Schubauer, G. B., and Dryden, H. L.: The Effect of Turbulence on the Drag of Flat Plates. NACA Rep. 546, 1935.

5. Hoerner, Sighard F.: Aerodynamic Drag. Publ. by the author (148 Busteed, Midland Park, N. J.), 1951.

6. Fage, A., and Warsap, J. H.: The Effects of Turbulence and Surface Roughness on the Drag of a Circular Cylinder. R. & M. No. 1283, British A.R.C., 1930.

7. Stephens, A. V.: Drag of Circular Cylinders in Flight. R. & M. No. 1892, British A.R.C., 1940.

TABLE I.- DRAG-FORCE READINGS IN POUNDS FOR EACH OF TWO BALANCES SUPPORTING TEST MODELS

(a) 6- by 72-inch plate

$\frac{r}{R}$	$\frac{z}{R}$ = 0.104		$\frac{z}{R}$ = 0.215		$\frac{z}{R}$ = 0.326		$\frac{z}{R}$ = 0.660		$\frac{z}{R}$ = 0.993		$\frac{z}{R}$ = 1.326	
	Balance A	Balance B	Balance A	Balance B	Balance A	Balance B	Balance A	Balance B	Balance A	Balance B	Balance A	Balance B
-0.333	1.37	1.87										
-.278	1.55	2.02	1.43	2.18	1.08	2.17						
-.222	1.54	2.26	1.52	2.33	1.57	2.30						
-.167	1.80	2.40	1.62	2.43	1.47	2.50						
-.111	1.84	2.21	1.82	2.18	1.62	2.53	2.10	2.80				
-.056	2.14	1.97	2.06	1.99	1.79	2.35						
0	2.38	1.63	2.30	1.87	2.26	1.99	2.29	2.36	2.51	2.52	2.48	7.75
.056	2.72	1.28	2.55	1.49	2.19	1.99						
.111	2.77	1.17	2.65	1.45	2.41	1.67	2.78	1.87	2.70	1.88	2.98	2.06
.167	2.63	1.05	2.65	1.30	2.53	1.45						
.222	2.48	1.03	2.40	1.20	2.48	1.35	2.95	1.62	2.80	1.58	2.87	1.99
.333	1.93	.94	2.01	.95	2.12	1.06	2.54	1.33	2.90	1.53	3.13	1.63
.444	1.41	.86	1.62	.86	1.84	.99	2.39	1.13	2.61	1.19	2.75	.84
.556	1.13	.80	1.23	.68	1.52	.72	2.23	.87	2.61	.91	2.76	.76
.667	1.00	.60	1.18	.53	1.53	.67	2.04	.54	2.60	.64	2.67	.51
.778	1.11	.45	1.28	.38	1.55	.40	2.18	.43	2.59	.39	2.76	.30
.889	1.22	.21	1.35	.19	1.68	.29	2.24	.28	2.59	.25	2.43	.02
1.000	1.45	.06	1.47	-.01	1.79	.01	2.09	-.01	2.46	-.05	2.49	-.04
1.111	1.51	-.12	1.61	-.10	1.79	-.08	2.07	-.18	2.20	-.28	2.26	-.19
1.222	1.69	-.27	1.71	-.25	1.93	-.25	2.13	-.31	2.13	-.26	2.15	-.28
1.333	1.60	-.34	1.66	-.32	1.79	-.34	1.96	-.39	1.93	-.35	1.49	-.34
1.444	1.41	-.38	1.51	-.38	1.47	-.42	1.88	-.36	1.32	-.34	.98	-.25
1.556	1.09	-.32	1.07	-.33	1.29	-.41	1.18	-.35	1.10	-.33	.58	-.22
1.667	.81	-.29	.67	-.25	.72	-.32	.45	-.20	.21	-.15	.37	-.15
1.778	.30	-.13	-.12	-.02	0	-.09	.06	-.10	.05	-.09	.15	-.08
1.889	-.12	.01	-.16	-.01	-.08	-.09	-.07	-.08	.02	-.05	.01	-.05
2.000	-.10	-.01	-.15	-.01	-.08	-.05	-.09	-.07	-.09	-.06	-.01	-.05
2.111	-.08	-.01	-.13	-.01	-.09	-.08	-.07	-.07				
2.222	-.05	-.01	-.05	-.05								

TABLE I.- DRAG-FORCE READINGS IN POUNDS FOR EACH OF TWO BALANCES SUPPORTING TEST MODELS - Continued

(b) 12- by 72-inch plate

$\frac{r}{R}$	$\frac{z}{R}$ = 0.104		$\frac{z}{R}$ = 0.215		$\frac{z}{R}$ = 0.326		$\frac{z}{R}$ = 0.660		$\frac{z}{R}$ = 0.993		$\frac{z}{R}$ = 1.326	
	Balance A	Balance B	Balance A	Balance B	Balance A	Balance B	Balance A	Balance B	Balance A	Balance B	Balance A	Balance B
0	5.35	4.21	5.07	4.34	5.10	4.21	4.80	4.57	4.57	4.36	4.81	4.27
.111	5.69	3.57	5.49	3.70	5.41	3.60	5.35	3.99	4.96	3.58	5.20	4.07
.222	4.87	2.79	5.15	3.01	5.01	2.72	4.81	3.43	4.50	3.19	4.81	3.22
.333	4.08	2.39	4.07	2.24	4.23	2.50	4.48	2.86	4.27	2.50	4.60	2.39
.444	3.25	1.90	3.16	1.60	3.55	1.93	4.30	2.66	4.08	2.23	4.76	2.32
.556	2.68	1.92	2.70	1.37	3.32	1.61	3.63	1.53	4.03	1.71	4.61	1.78
.667	2.54	1.63	2.57	.99	3.08	1.01	4.29	1.66	3.75	.83	4.56	1.03
.778	2.66	.94	2.65	.66	2.99	.69	4.14	.81	3.94	.41	4.80	.83
.889	2.99	.40	3.07	.43	3.37	.37	4.08	.23	3.99	.24	3.84	-.04
1.000	3.51	.11	3.26	.05	3.29	-.02	3.75	-.24	4.43	.04	4.87	.22
1.111	3.83	-.28	3.46	-.27	3.54	-.36	3.66	-.47	3.95	-.37	3.65	-.63
1.222	4.02	-.57	3.55	-.54	3.46	-.61	3.92	-.59	3.60	-.61	3.50	-.66
1.333	3.53	-.82	3.35	-.69	3.14	-.75	3.27	-.74	2.43	-.67	2.83	-.76
1.444	3.34	-.92	3.04	-.78	2.79	-.83	2.77	-.76	3.11	-.64	2.17	-.72
1.556	2.67	-.82	2.42	-.75	2.22	-.77	1.46	-.57	1.64	-.54	.91	-.43
1.667	1.44	-.62	1.35	-.55	1.12	-.53	.18	-.26	.13	-.15	.34	-.24
1.778	.21	-.33	-.17	-.14	-.12	-.09	0	-.10	.05	-.11	.05	-.15
1.889	-.38	-.08	-.06	-.18	-.11	-.09	-.09	-.09	-.05	-.05	-.06	-.14
2.000	-.32	-.09	-.10	-.16	-.12	-.11	-.09	-.10	-.06	-.07	-.09	-.14
2.111	-.18	-.08	-.13	-.05	-.11	-.07	-.09	-.07			-.09	-.07
2.222	-.07	-.06			-.08	-.04						

TABLE I.- DRAG-FORCE READINGS IN POUNDS FOR EACH OF TWO BALANCES

SUPPORTING TEST MODELS - Continued

(c) 12- by 72-inch plate; extended traverse range

$\frac{r}{R}$	$\frac{z}{R}$ = 0.104		$\frac{z}{R}$ = 0.215		$\frac{z}{R}$ = 0.326		$\frac{z}{R}$ = 0.660		$\frac{z}{R}$ = 0.993		$\frac{z}{R}$ = 1.326	
	Balance A	Balance B	Balance A	Balance B	Balance A	Balance B	Balance A	Balance B	Balance A	Balance B	Balance A	Balance B
-0.333	3.54	4.42	3.54	4.58	3.70	4.85	2.85	4.90	3.10	4.79	3.86	5.22
-.222	3.78	5.13	3.86	5.24	3.96	5.20	3.00	5.32	4.15	5.38	3.97	5.17
-.167	4.15	5.46	4.20	5.47	4.35	5.37	3.83	5.48	4.42	5.28	4.31	5.12
-.111	4.38	5.45	4.41	5.29	4.54	5.39	3.84	5.46	4.37	5.08	4.59	4.93
-.056	4.73	5.06	4.73	4.83	4.67	4.92	3.92	5.21	4.86	4.90	4.69	4.73
0	5.20	4.52	4.99	4.43	5.07	4.61	4.67	5.35	4.76	4.64	4.83	4.37
.056	5.54	4.14	5.32	3.99	5.31	4.22	4.83	5.23	4.81	4.69	4.55	4.21
.111	5.69	3.77	5.61	3.75	5.51	3.66	5.10	4.98	4.93	4.74	4.44	4.11
.167	5.46	3.35	5.59	3.22	5.40	3.24	5.12	4.65	4.85	4.50	4.22	3.03
.222	5.03	3.00	5.30	2.96	5.25	3.16	5.34	4.38	4.64	4.25	4.61	3.35
.333	4.23	2.30	4.54	2.59	4.48	2.52	5.15	3.96	4.39	3.52	4.39	2.34
.444	3.17	1.80	3.61	2.08	3.60	1.93	4.92	3.37	4.39	3.02	4.37	2.32
.556	2.78	1.64	2.96	1.78	3.16	1.56	4.56	2.74	4.27	2.05	4.17	1.34
.667	2.43	1.22	2.69	1.21	3.00	1.13	4.33	1.89	4.47	1.40	4.12	.93

TABLE I.- DRAG-FORCE READINGS IN POUNDS FOR EACH OF TWO BALANCES SUPPORTING TEST MODELS - Continued

(d) 6-inch cylinder

$\frac{r}{R}$	$\frac{z}{R}$ = 0.195		$\frac{z}{R}$ = 0.306		$\frac{z}{R}$ = 0.416		$\frac{z}{R}$ = 0.750		$\frac{z}{R}$ = 1.083	
	Balance A	Balance B	Balance A	Balance B	Balance A	Balance B	Balance A	Balance B	Balance A	Balance B
-0.333	0.37	0.76	0.31	0.69	0.30	0.80	0.32	1.01	0.32	1.04
-.222	.37	1.00	.31	.89	.37	.96	.45	.95	.49	1.00
-.167	.37	1.07	.38	.88	.46	.93	.54	.87	.48	.90
-.111	.50	1.03	.50	.82	.45	.84	.70	.80	.63	.82
-.056	.54	1.03	.57	.74	.64	.70	.77	.73	.69	.79
0	.73	.88	.65	.65	.71	.71	.77	.67	.82	.64
.056	.78	.82	.73	.60	.80	.59	.81	.57	.92	.55
.111	.88	.59	.81	.48	.80	.46	.90	.49	.89	.51
.167	.87	.61	.74	.36	.81	.42	.93	.37	.91	.43
.222	.82	.52	.74	.40	.79	.41	.89	.36	.97	.36
.333	.62	.45	.52	.33	.71	.33	.83	.28	.89	.27
.444	.45	.47	.49	.30	.53	.27	.78	.23	.79	.18
.556	.35	.42	.36	.27	.33	.25	.74	.15	.79	.12
.667	.35	.38	.32	.27	.38	.23	.71	.13	.78	.10
.778	.35	.31	.36	.18	.35	.20	.75	0	.85	.02
.889	.44	.24	.36	.13	.48	.10	.68	.03	.77	-.01
1.000	.51	.18	.48	.06	.51	.05	.72	-.03	.72	-.08
1.111	.63	.13	.58	.01	.58	-.01	.67	-.10	.69	-.10
1.222	.76	.03	.73	-.10	.73	-.10	.74	-.13	.73	-.17
1.333	.76	-.04	.75	-.13	.70	-.19	.66	-.16	.64	-.18
1.444	.74	-.08	.67	-.17	.67	-.19	.45	-.17	.50	-.17
1.556	.61	-.07	.52	-.19	.54	-.17	.35	-.15	.48	-.10
1.667	.39	-.07	.35	-.17	.25	-.14	.09	-.09	-.05	-.05
1.778	.12	-.03	.04	-.12	-.01	-.03	-.02	-.02	-.02	-.03
1.889	-.05	0	-.04	.01	-.01	-.01	-.02	-.01	-.02	-.03
2.000	-.04	.01	-.03	-.02	-.02	-.01	-.01	-.01	-.02	-.03
2.111	-.02	.01	-.04	-.02						
2.222	-.01	0	-.01	0						

TABLE I.- DRAG-FORCE READINGS IN POUNDS FOR EACH OF TWO BALANCES

SUPPORTING TEST MODELS - Continued

(e) 6-inch cylinder with strips on center line

0.130-inch-diameter strip										
$\frac{r}{R}$	$\frac{z}{R}$ = 0.195		$\frac{z}{R}$ = 0.306		$\frac{z}{R}$ = 0.416		$\frac{z}{R}$ = 0.750		$\frac{z}{R}$ = 1.083	
	Balance A	Balance B	Balance A	Balance B	Balance A	Balance B	Balance A	Balance B	Balance A	Balance B
-0.333			0.73	1.29	0.80	1.56	0.83	1.97	0.76	2.03
-.222			.77	1.58	.91	1.71	1.04	2.04	1.08	2.08
-.167	0.90	1.96	.83	1.61	1.08	1.63	1.15	1.83	1.28	1.99
-.111	1.01	1.96	.98	1.55	1.12	1.66	1.40	1.75	1.28	1.85
-.056	1.17	1.86	1.18	1.38	1.34	1.45	1.60	1.63	1.50	1.69
0	1.39	1.61	1.39	1.14	1.50	1.20	1.75	1.44	1.75	1.56
.056	1.57	1.43	1.50	1.05	1.62	1.03	1.79	1.15	1.85	1.38
.111	1.66	1.27	1.65	.96	1.60	.92	1.89	1.13	1.95	1.36
.167	1.69	1.16	1.66	.78	1.61	.81	1.97	.91	2.08	.97
.222			1.54	.70	1.47	.70	1.97	.86	1.94	1.02
.333			1.34	.68	1.41	.68	1.97	.73	1.99	.66
.444			.92	.55	1.19	.55	1.72	.59	1.82	.50
.556			.83	.52	.97	.52			1.74	.40
.667			.74	.47					1.65	.30
.778			.81	.29					1.72	.19
.889	.91	.44	.99	.16					1.58	-.02
1.000	1.03	.31	1.16	.06					1.50	-.12
1.111	1.18	.17							1.47	-.22

0.0625-inch-diameter strip					0.007-inch by 0.5-inch tape strip	
$\frac{r}{R}$	$\frac{z}{R}$ = 0.195		$\frac{z}{R}$ = 0.416		$\frac{z}{R}$ = 0.416	
	Balance A	Balance B	Balance A	Balance B	Balance A	Balance B
-0.167	0.72	1.66	0.80	1.38	0.40	0.80
-.111	.87	1.64	.83	1.27	.51	.73
-.056	.94	1.56	1.05	1.17	.57	.69
0	1.06	1.40	1.12	1.03	.65	.54
.056	1.26	1.22	1.32	.89	.73	.49
.111	1.26	1.08	1.33	.80	.80	.38
.167	1.24	.97	1.32	.68	.85	.30
.889	.68	.44	.91	.17	.43	.11
1.000	.84	.32	1.00	.04	.51	.02
1.111	.98	.20	1.08	-.07	.68	-.03

TABLE I.- DRAG-FORCE READINGS IN POUNDS FOR EACH OF TWO BALANCES SUPPORTING TEST MODELS - Continued

(f) 12-inch cylinder

$\frac{r}{R}$	$\frac{z}{R}$ = 0.278		$\frac{z}{R}$ = 0.389		$\frac{z}{R}$ = 0.500		$\frac{z}{R}$ = 0.833		$\frac{z}{R}$ = 1.167	
	Balance A	Balance B	Balance A	Balance B	Balance A	Balance B	Balance A	Balance B	Balance A	Balance B
-0.333	0.87	2.31	0.71	2.05	0.67	2.43	0.78	2.54	0.59	2.63
-.222	.90	2.77	.83	2.52	1.02	2.49	1.05	2.54	.85	2.62
-.111	1.46	2.53	1.18	3.39	1.15	2.53	1.33	2.31	1.17	2.17
0	1.81	1.93	1.57	2.03	1.70	2.14	1.84	1.72	1.64	1.81
.111	2.14	1.49	1.94	1.52	2.13	1.66	2.07	1.40	2.19	1.38
.222	2.10	1.27	2.07	1.11	2.29	1.32	2.18	1.17	2.10	1.03
.333	1.91	1.04	1.70	1.82	2.02	1.08	2.04	.80	2.17	.82
.444	1.51	1.09	1.56	.94	2.03	.83	2.21	.77	1.94	.80
.556	1.32	.85	1.45	.81	1.87	.79	2.12	.56	1.85	.31
.667	1.12	.71	1.31	.66	1.54	.58	1.86	.31	1.76	.09
.778	1.19	.53	1.39	.43	1.65	.35	1.81	-.05	1.69	-.02
.889	1.37	.29	1.55	.23	1.73	.25	1.99	-.19	1.82	-.02
1.000	1.56	.19	1.82	-.03	1.80	.03	1.91	-.07	1.90	-.04
1.111	1.93	-.04	1.85	-.17	1.96	-.28	2.08	-.33	1.78	-.39
1.222	2.05	-.35	1.97	-.31	2.04	-.41	2.02	-.50	1.45	-.49
1.333	2.08	-.43	1.78	-.45	1.95	-.45	1.60	-.46	1.13	-.47
1.444	1.88	-.54	1.76	-.53	1.71	-.58	1.16	-.45	.76	-.44
1.556	1.52	-.59	1.31	-.53	1.17	-.50	.66	-.38	.20	-.19
1.667	1.06	-.48	.62	-.44	.71	-.41	.19	-.17	0	-.09
1.778	.19	-.25	-.12	-.14	-.02	-.07	.02	-.07	-.02	-.10
1.889	-.14	-.05	-.07	-.06	-.08	-.06	0	-.06	-.02	-.05
2.000	-.09	-.04	-.10	-.05	-.06	-.03	-.02	-.06	-.02	-.03
2.111	-.09	-.06	-.06	-.06	-.05	-.03	-.03	-.05	-.02	-.04
2.222	-.04	-.04	-.04	-.03	-.02	-.02	-.03	-.05	-.04	-.05

TABLE I:- DRAG-FORCE READINGS IN POUNDS FOR EACH OF TWO BALANCES SUPPORTING TEST MODELS - Concluded

(g) 12-inch cylinder with strip

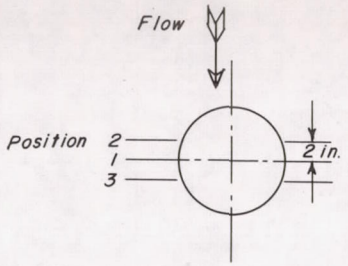

$\frac{r}{R}$	Position 1 $\frac{z}{R}$ = 0.278		Position 1 $\frac{z}{R}$ = 0.500		Position 1 $\frac{z}{R}$ = 1.167		Position 2 $\frac{z}{R}$ = 0.278		Position 2 $\frac{z}{R}$ = 0.500		Position 3 $\frac{z}{R}$ = 0.500	
	Balance A	Balance B	Balance A	Balance B	Balance A	Balance B	Balance A	Balance B	Balance A	Balance B	Balance A	Balance B
-0.333	1.15	3.12	1.65	3.59	1.14	3.76	0.73	2.75	1.20	3.06	0.87	3.06
-.222	1.54	3.45	1.55	3.93	1.63	3.91	1.32	3.16	1.05	3.30	1.06	3.16
-.111	1.93	3.68	2.24	3.78	2.22	3.57	1.71	2.90	2.08	2.97	1.55	3.18
0	2.42	3.14	3.11	2.95	2.56	3.32	2.05	2.60	2.37	2.74	2.09	2.72
.111	3.15	2.10	3.31	2.46	3.04	2.93	2.64	1.67	2.83	2.10	2.58	2.18
.222	3.15	1.93	3.31	1.72	3.48	2.29	2.68	1.38	2.86	1.81	2.72	1.81
.333	2.62	1.68	3.21	1.72	3.39	1.80	2.15	1.33	2.64	1.32	2.77	1.35
.444	2.27	1.50	2.50	1.33	3.44	1.60	1.78	1.18	2.44	1.10	2.77	1.10
.556	1.91	1.27	2.46	1.11	3.53	1.06	1.54	1.03	2.22	.92	2.33	.87
.667			2.55	1.06								
.778			2.54	.49								
.889			2.74	.20								
1.000			2.94	-.08								
1.111			2.86	-.32								
1.222			2.83	-.46								
1.333			2.27	-.59								
1.444			2.00	-.64								
1.556			1.35	-.57								
1.667			.81	-.46								
1.778			-.06	-.13								
1.889			-.07	-.05								
2.000			-.05	-.04								
2.111			-.08	-.08								
2.222			-.05	-.05								

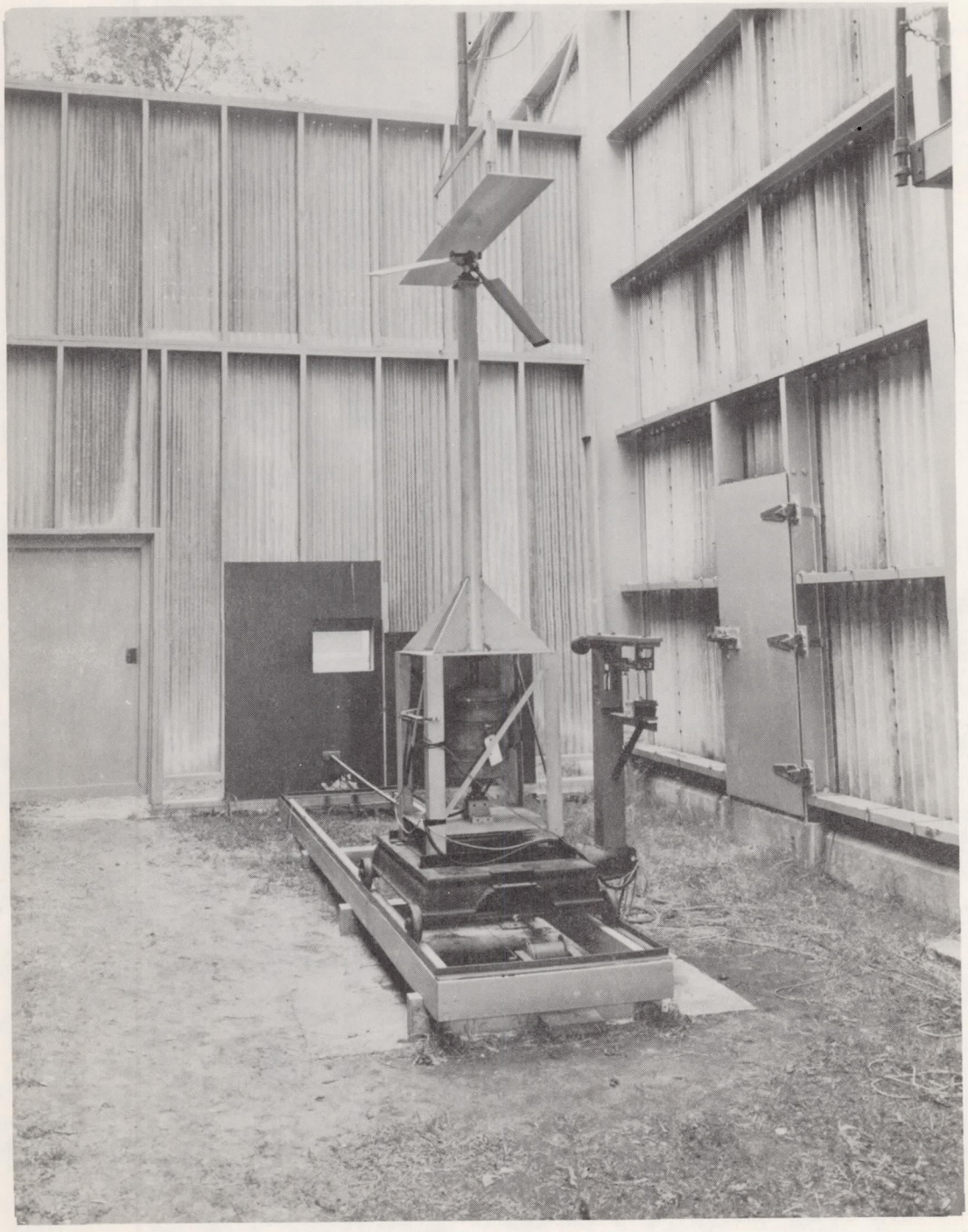

L-95636

Figure 1.- The apparatus with the 12- by 72-inch flat plate mounted on drag balances.

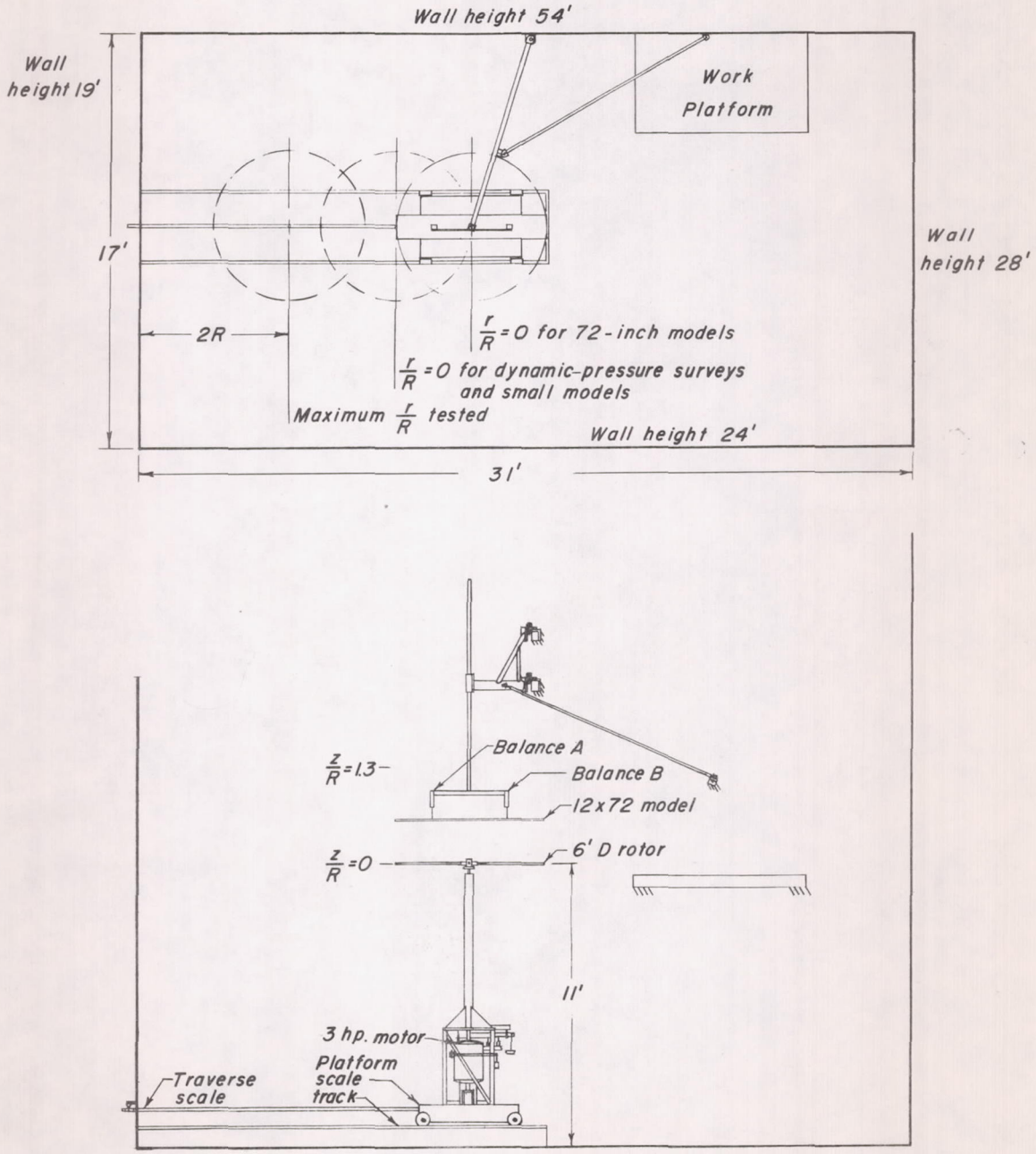

Figure 2.- Location of apparatus, models, and slipstream survey devices in test area.

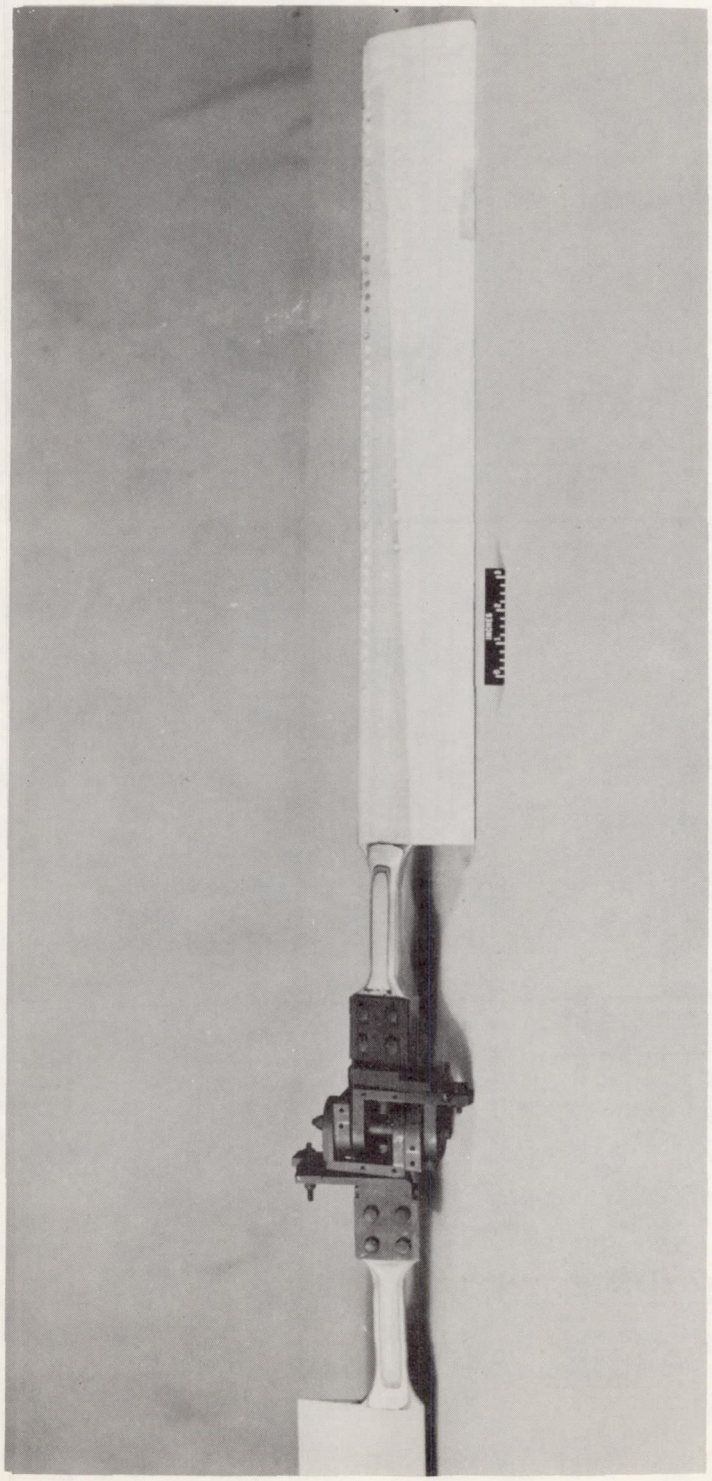

L-57-2238

Figure 3.- Rotor.

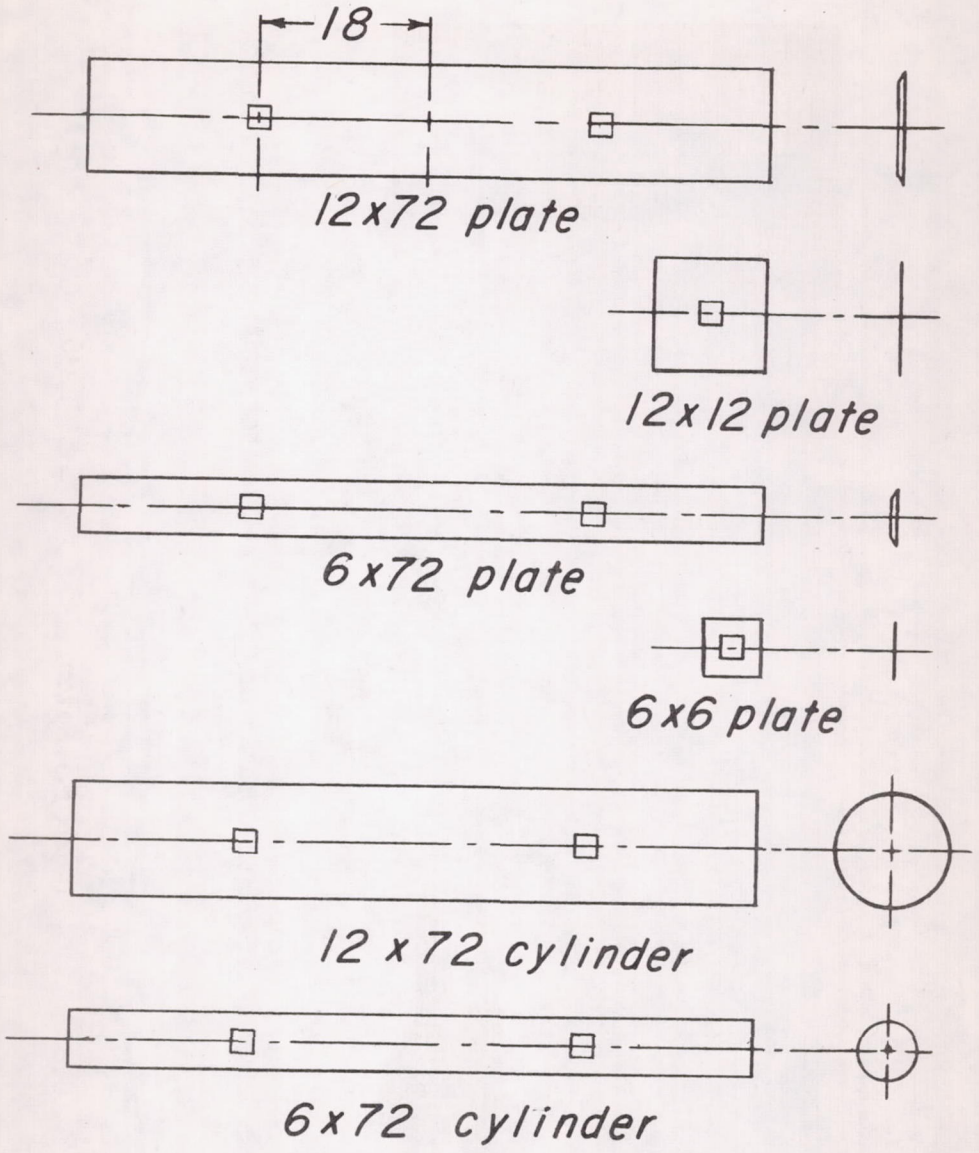

Figure 4.- Models tested. All dimensions are in inches.

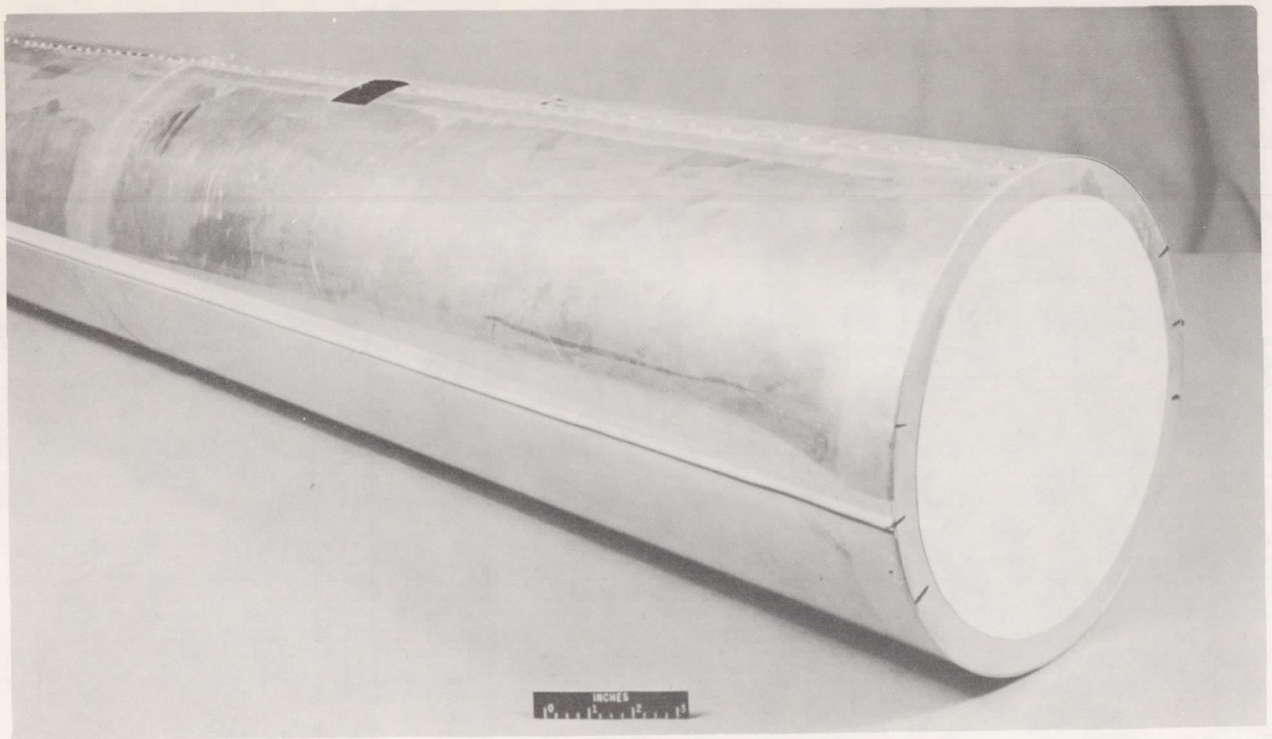

(a) 0.130-inch-diameter strip taped on 12-inch-diameter cylinder.

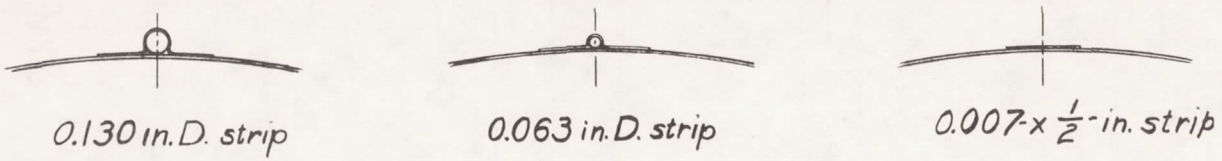

(b) Sketch of the three strips used. L-57-2241

Figure 5.- Details of strips used in cylinder tests.

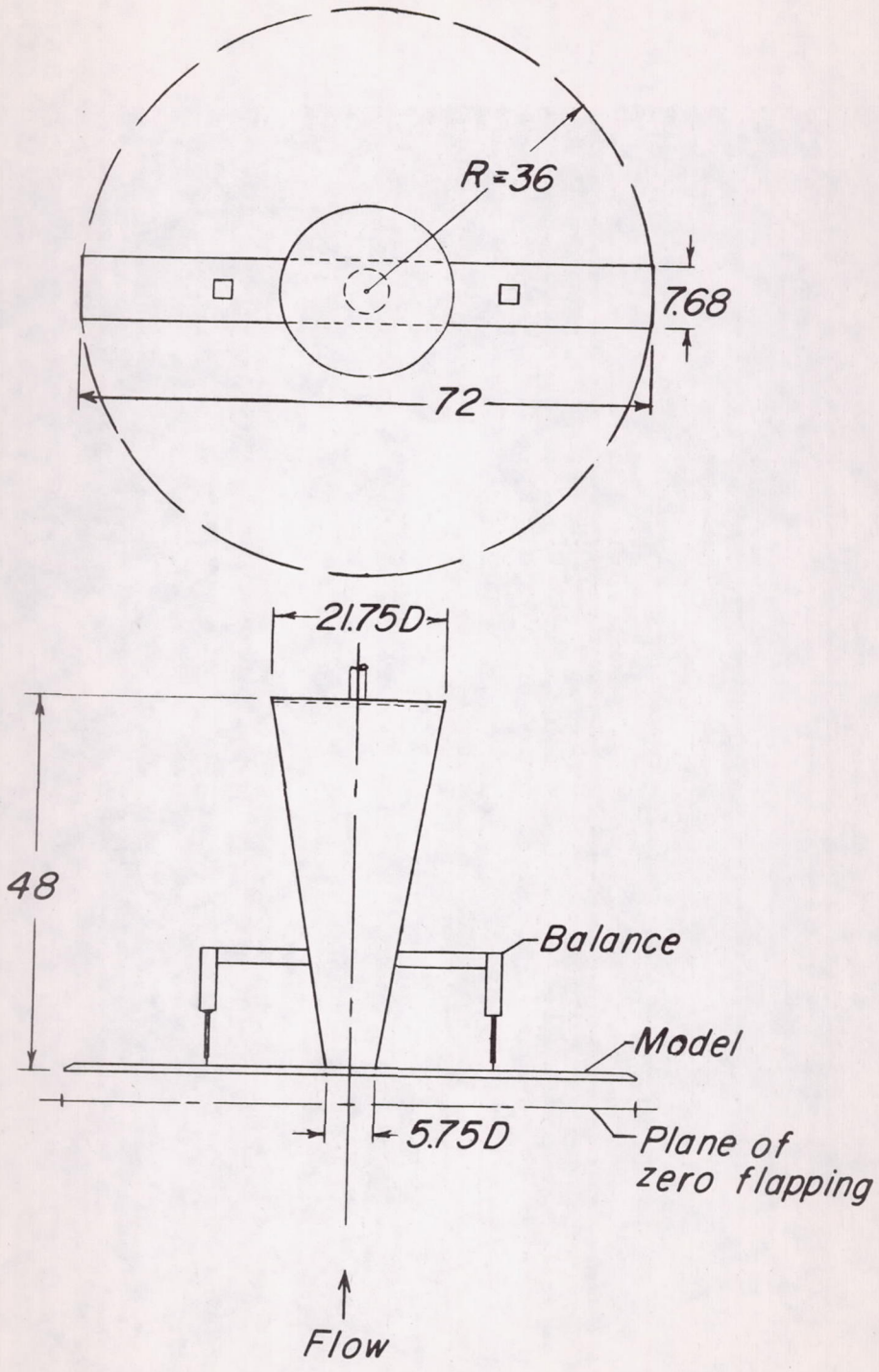

Figure 6.- Model of Langley helicopter tower and flat plate in test position. z/R = 0.104. All dimensions are in inches.

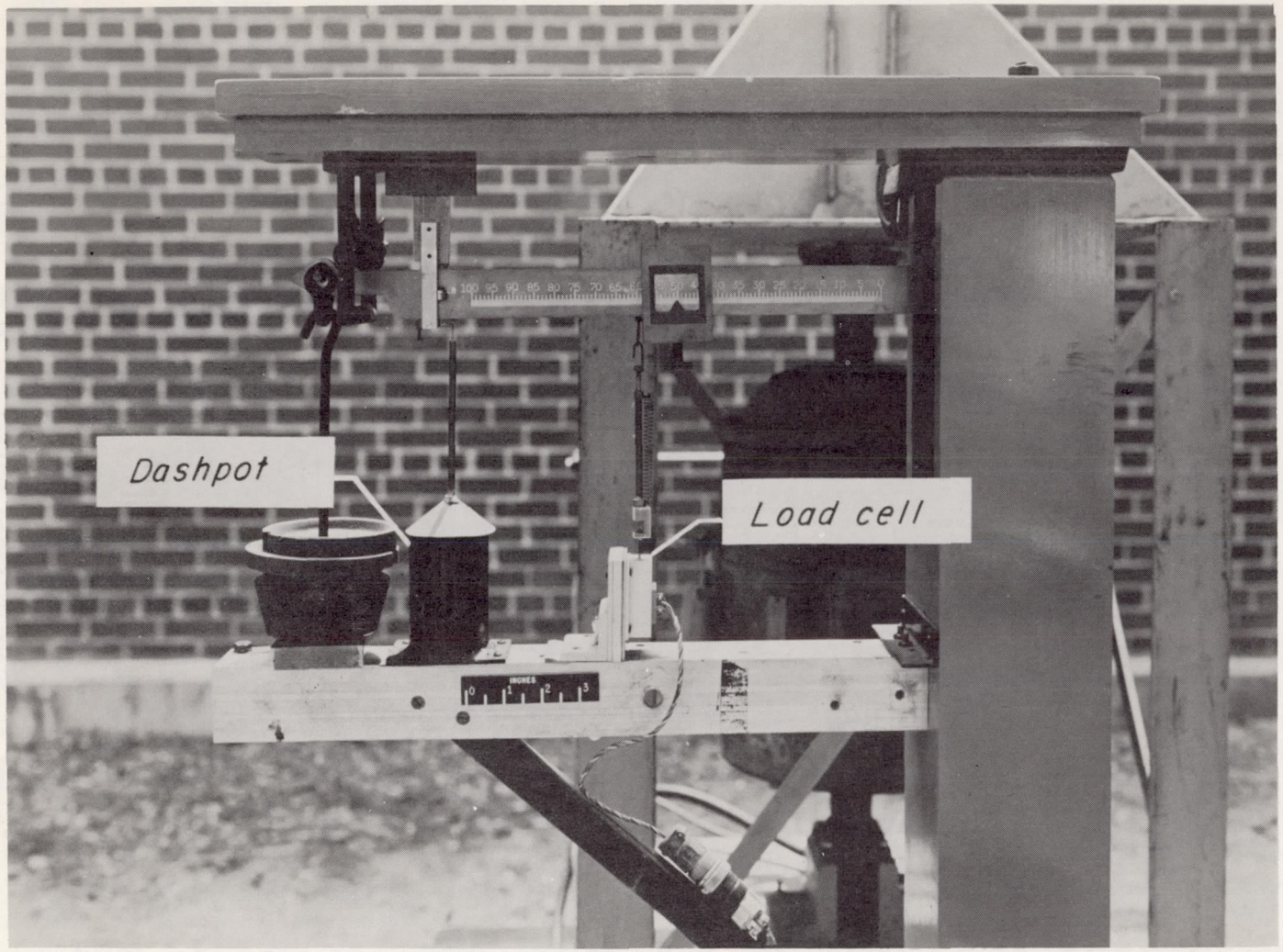

L-57-2430.1

Figure 7.- Load cell and dashpot installation on platform scale beam.

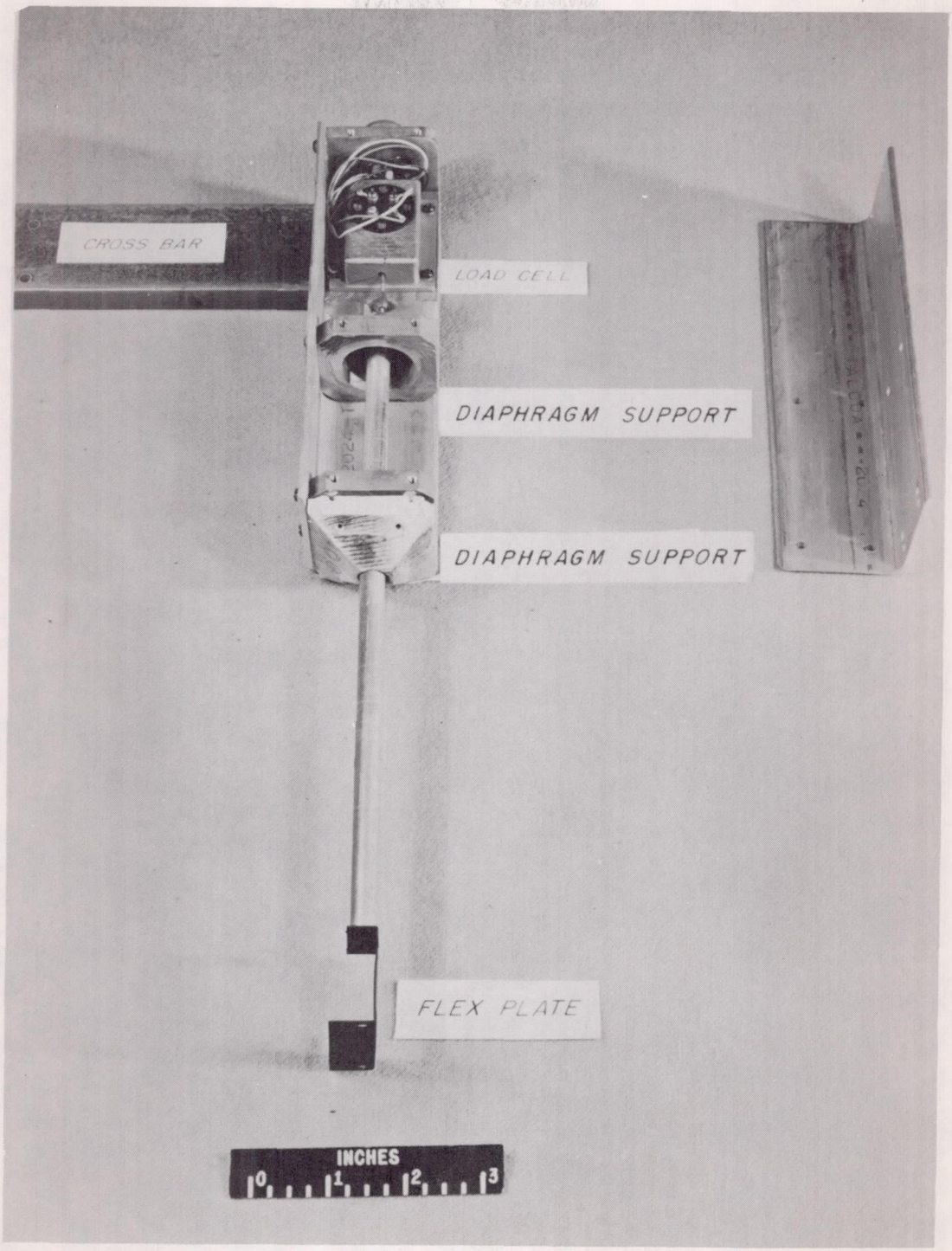

Figure 8.- Drag balance with case open. L-57-2243.1

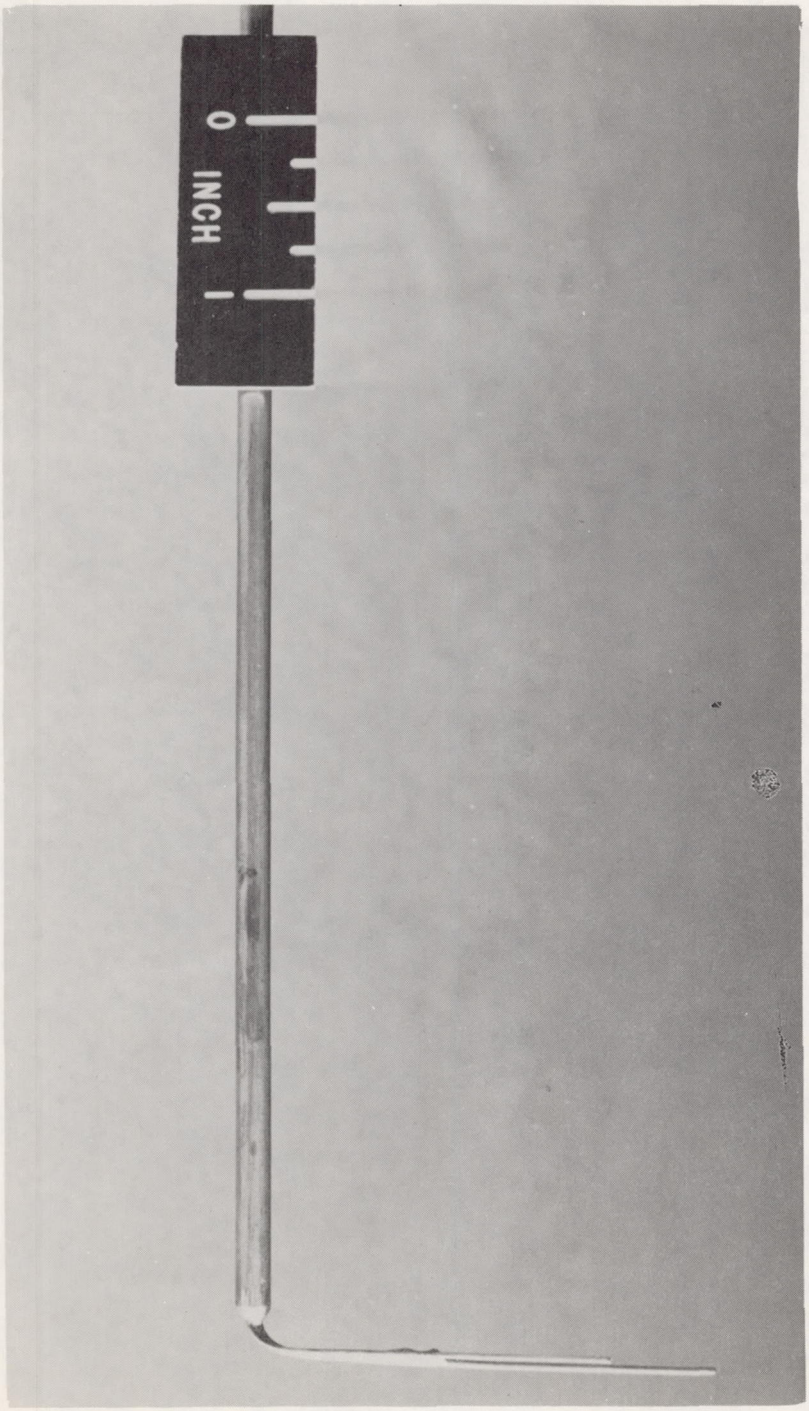

Figure 9.- Pitot-static tube. L-57-2244

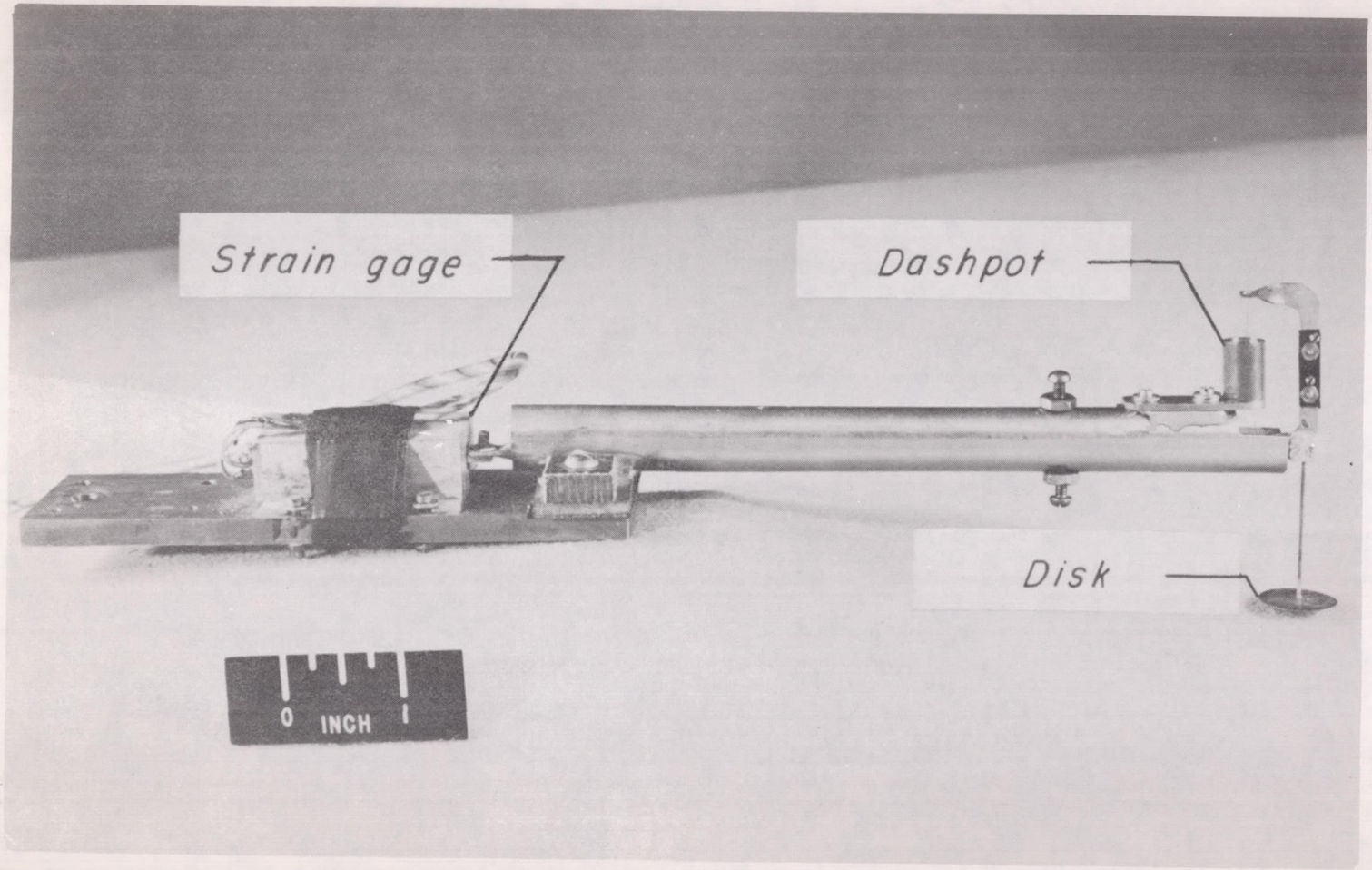

L-57-2242.1

Figure 10.- Slipstream survey device with 0.71-inch-diameter disk.

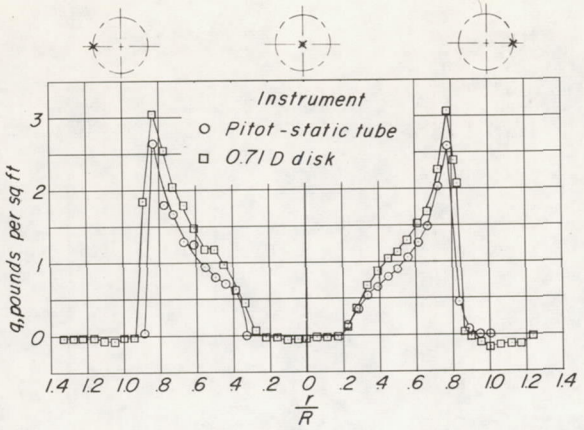

(a) z/R = 0.104.

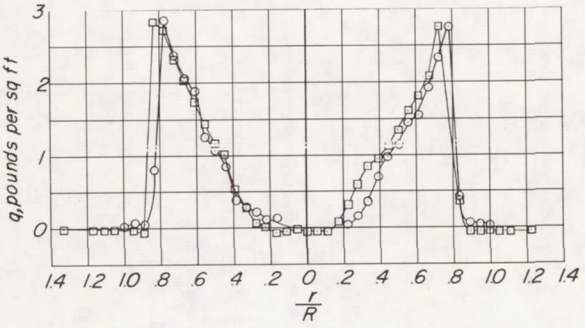

(b) z/R = 0.215.

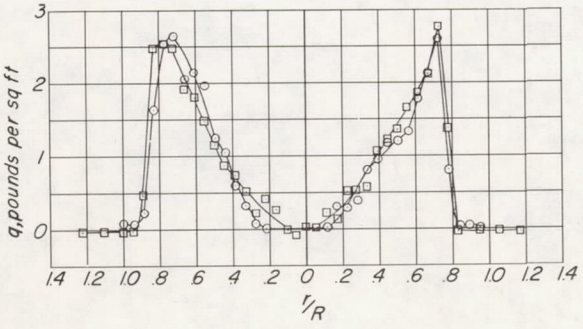

(c) z/R = 0.326.

Figure 11.- Slipstream dynamic pressure profiles at various distances from the plane of zero flapping.

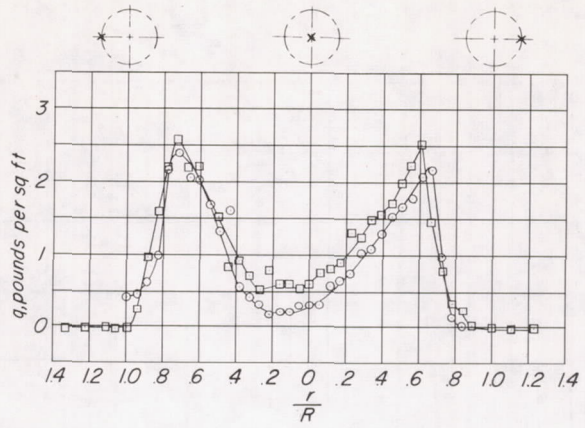

(d) z/R = 0.660.

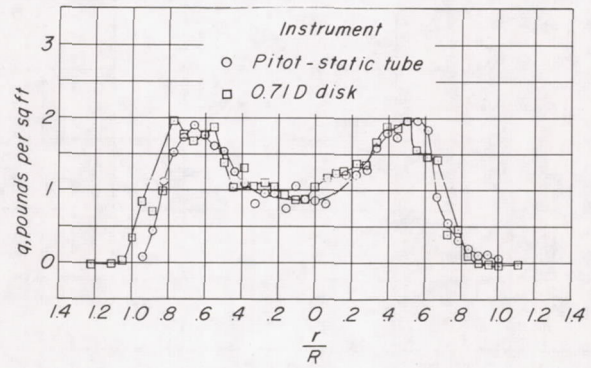

(e) z/R = 0.993.

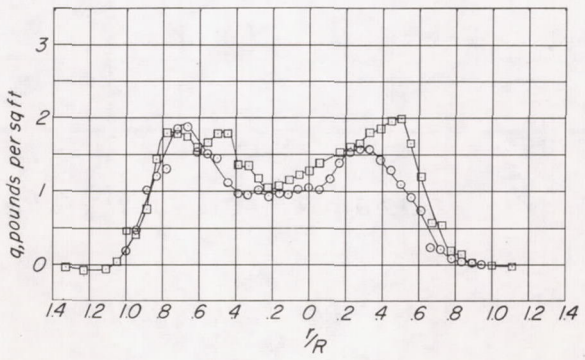

(f) z/R = 1.326.

Figure 11.- Concluded.

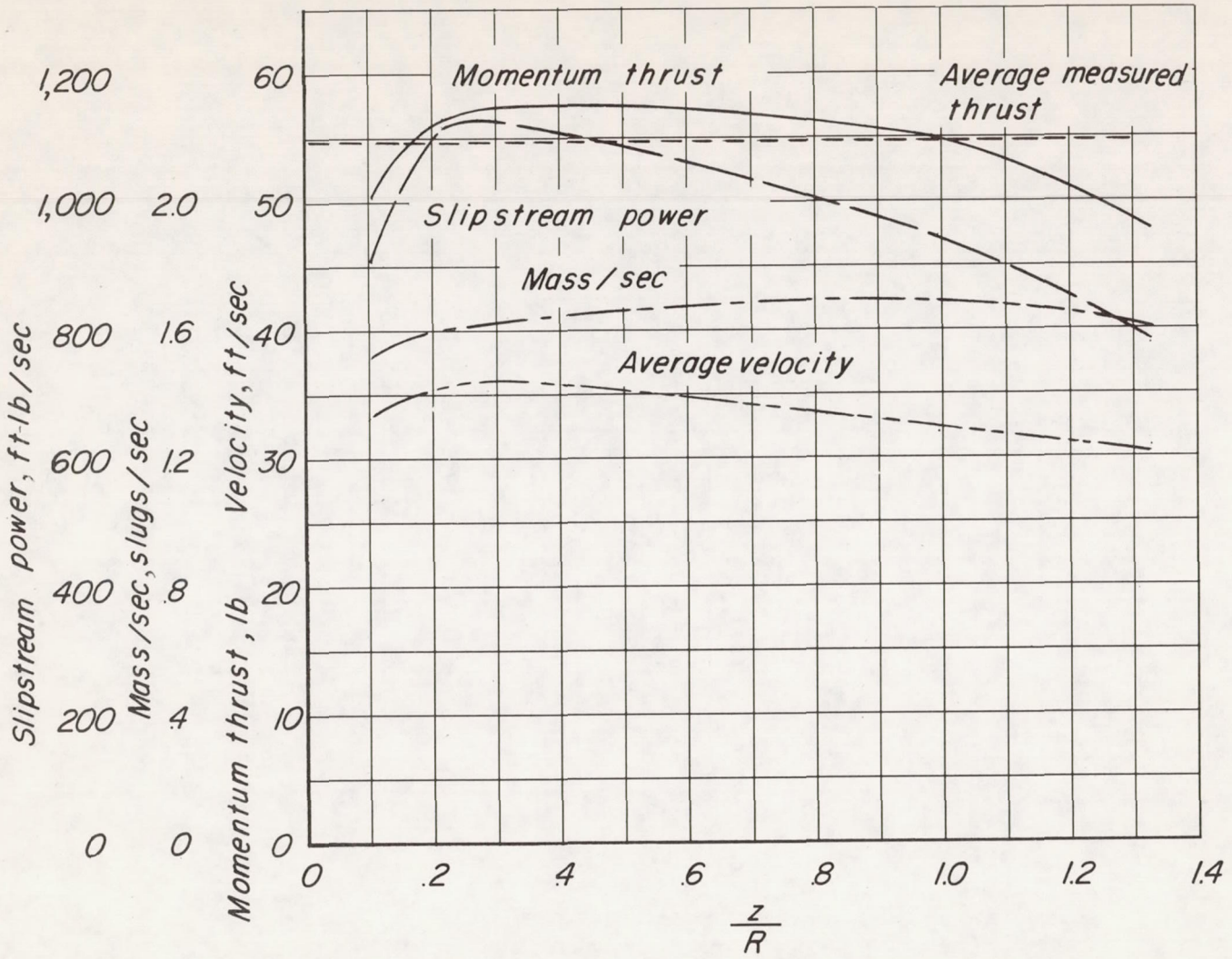

Figure 12.- Momentum thrust, slipstream power, mass flow, and average velocity obtained from integrations of the slipstream surveys.

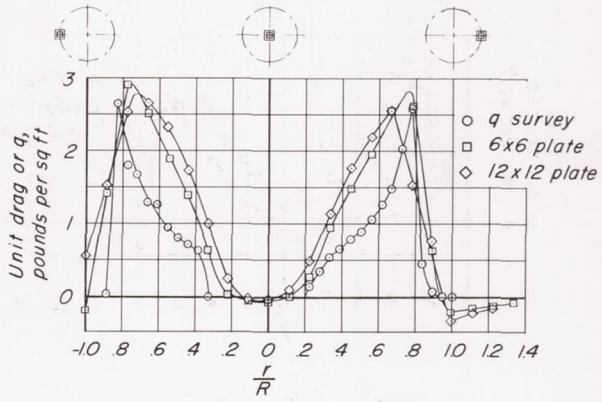

(a) z/R = 0.104.

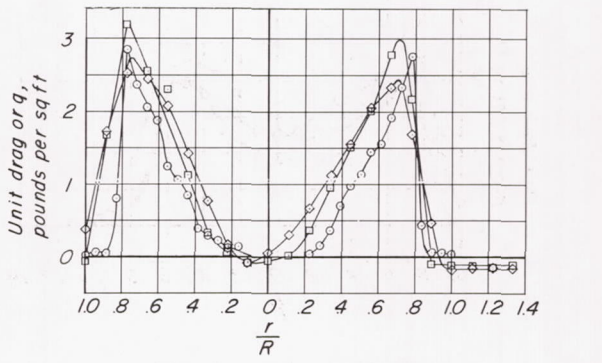

(b) z/R = 0.215.

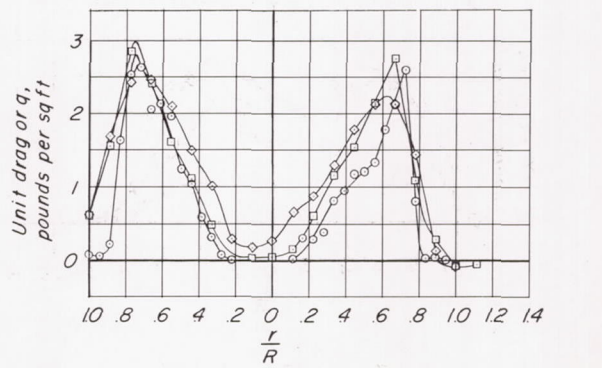

(c) z/R = 0.326.

Figure 13.- Variation of drag of square plates with lateral position for various distances from the rotor plane of zero flapping.

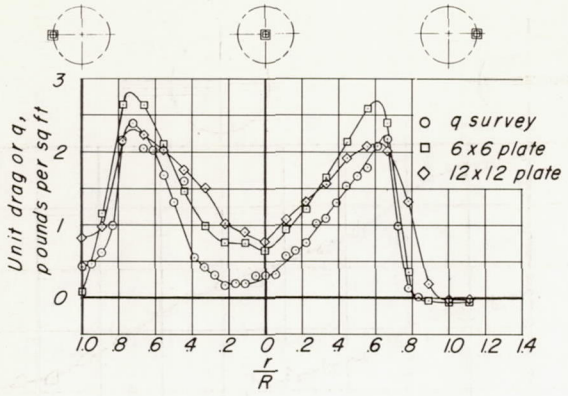

(d) z/R = 0.660.

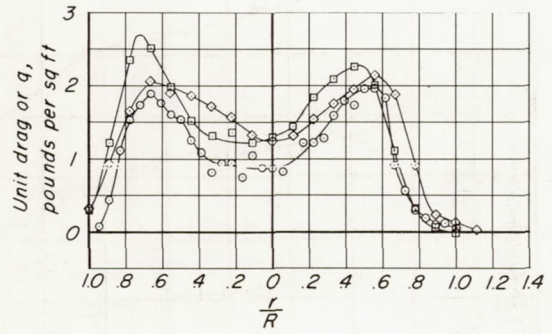

(e) z/R = 0.993.

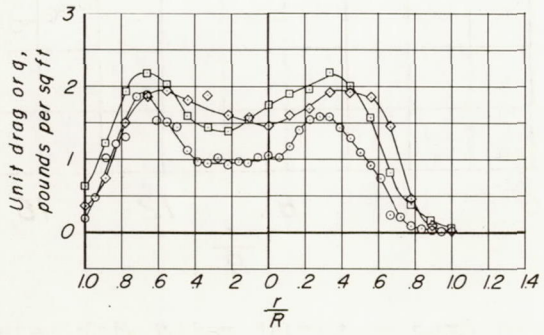

(f) z/R = 1.326.

Figure 13.- Concluded.

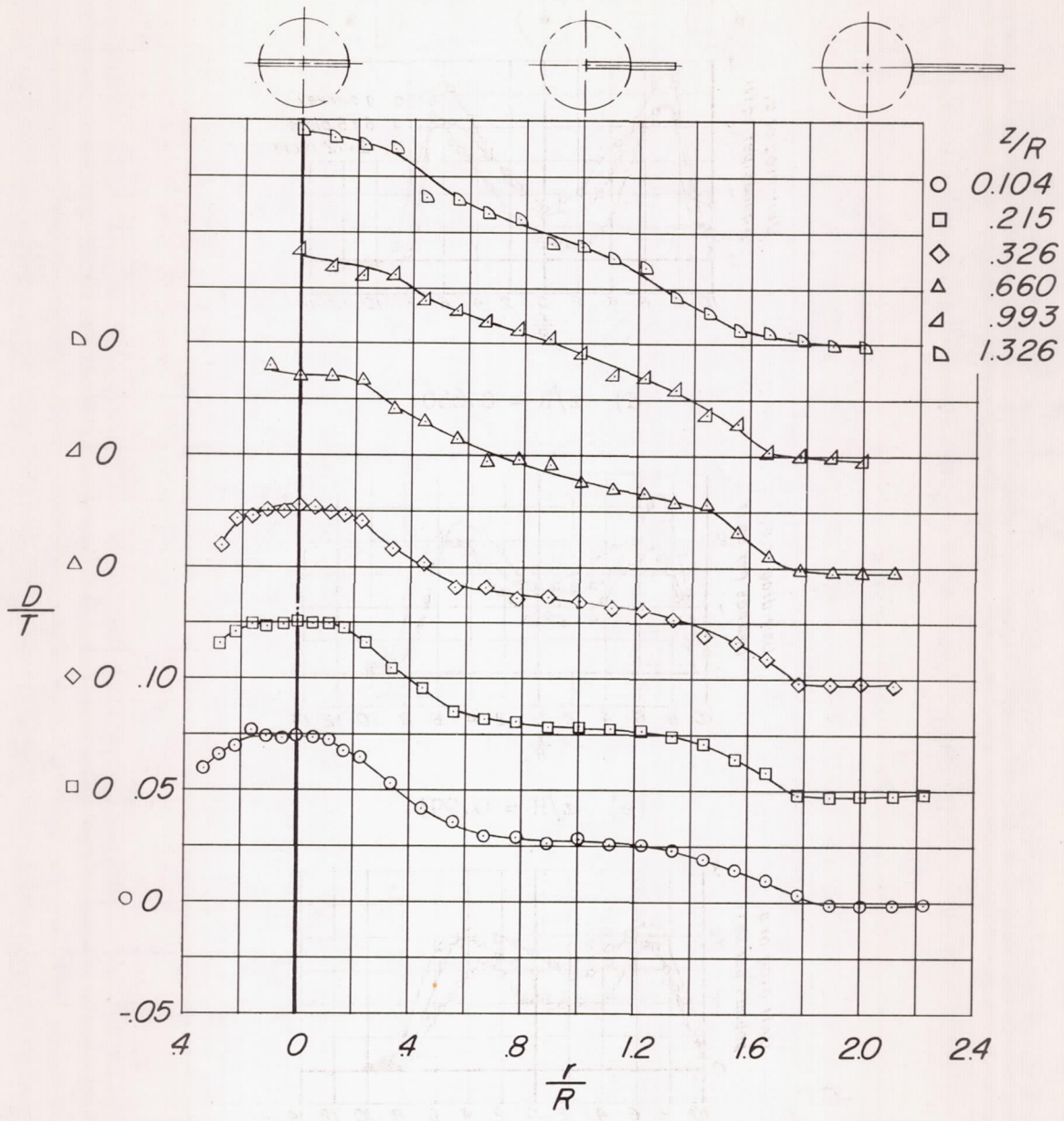

Figure 14.- Variation of drag-to-thrust ratio with lateral position of model for various distances from the rotor plane of zero flapping. 6- by 72-inch plate.

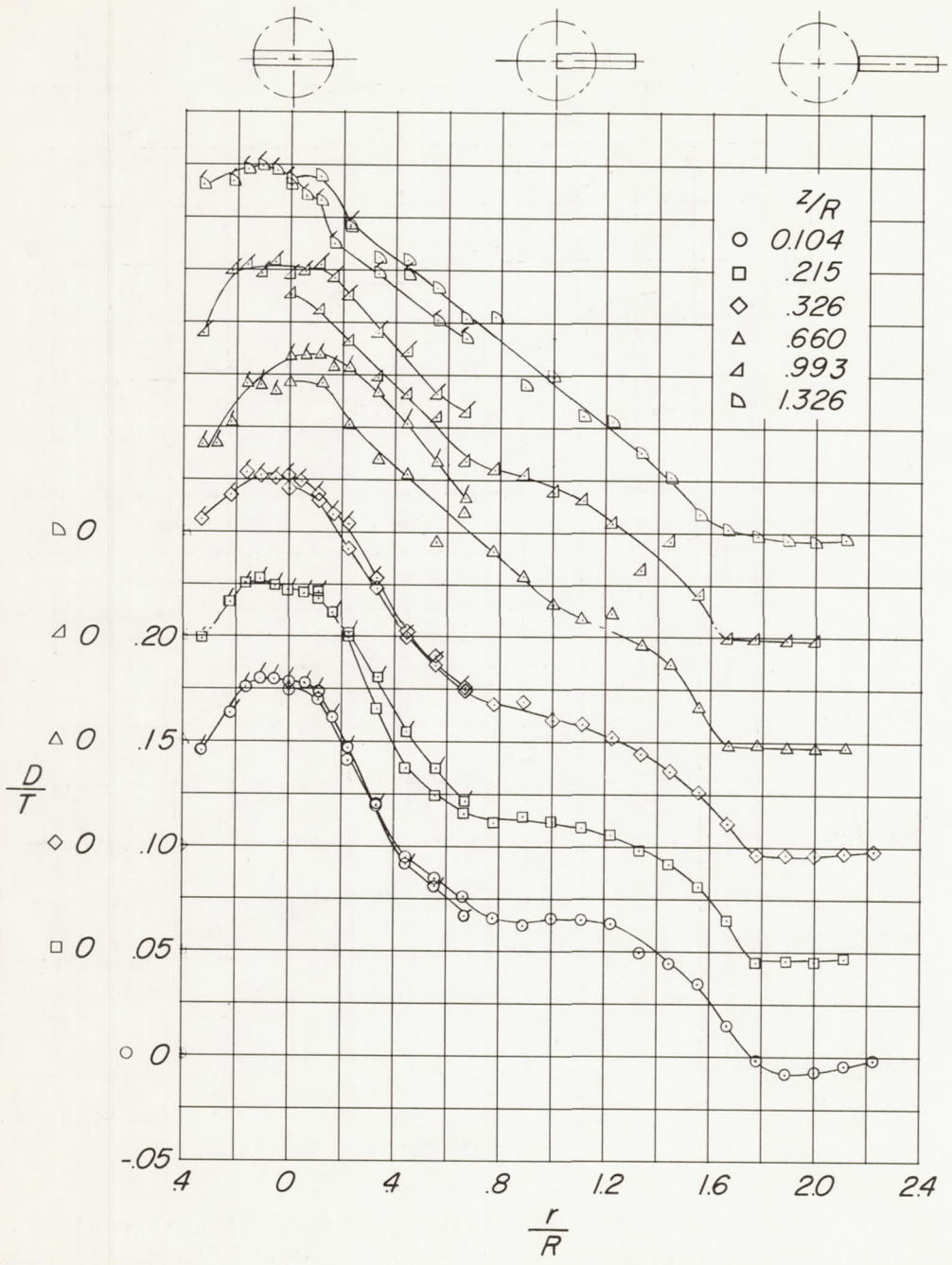

Figure 15.- Variation of drag-to-thrust ratio with lateral position of model for various distances from the rotor plane of zero flapping. 12- by 72-inch plate. Repeat runs made to extend the traverse range are designated with flags.

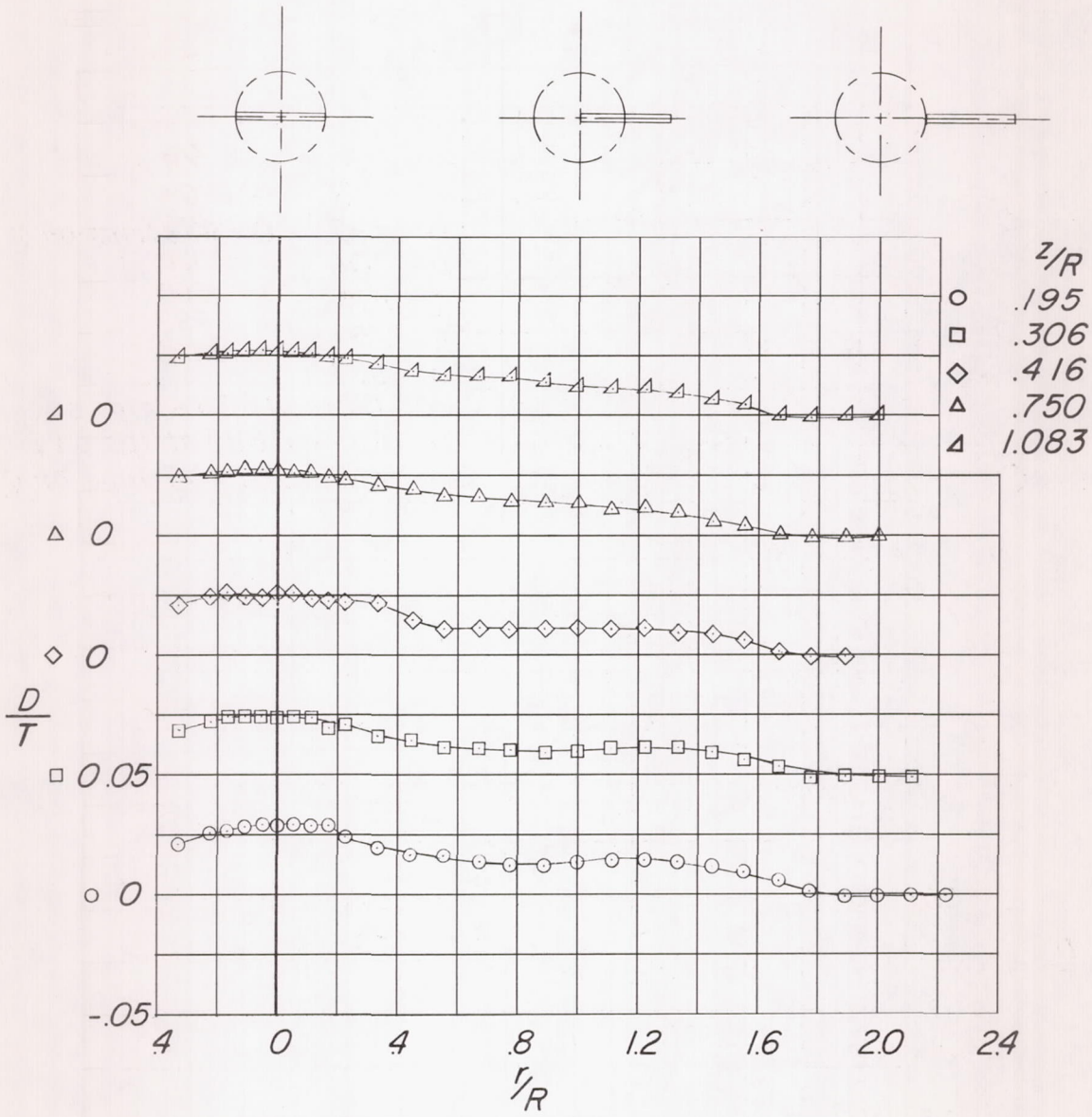

(a) 6-inch cylinder.

Figure 16.- Variation of drag-to-thrust ratio with lateral position of model for various distances from the rotor plane of zero flapping.

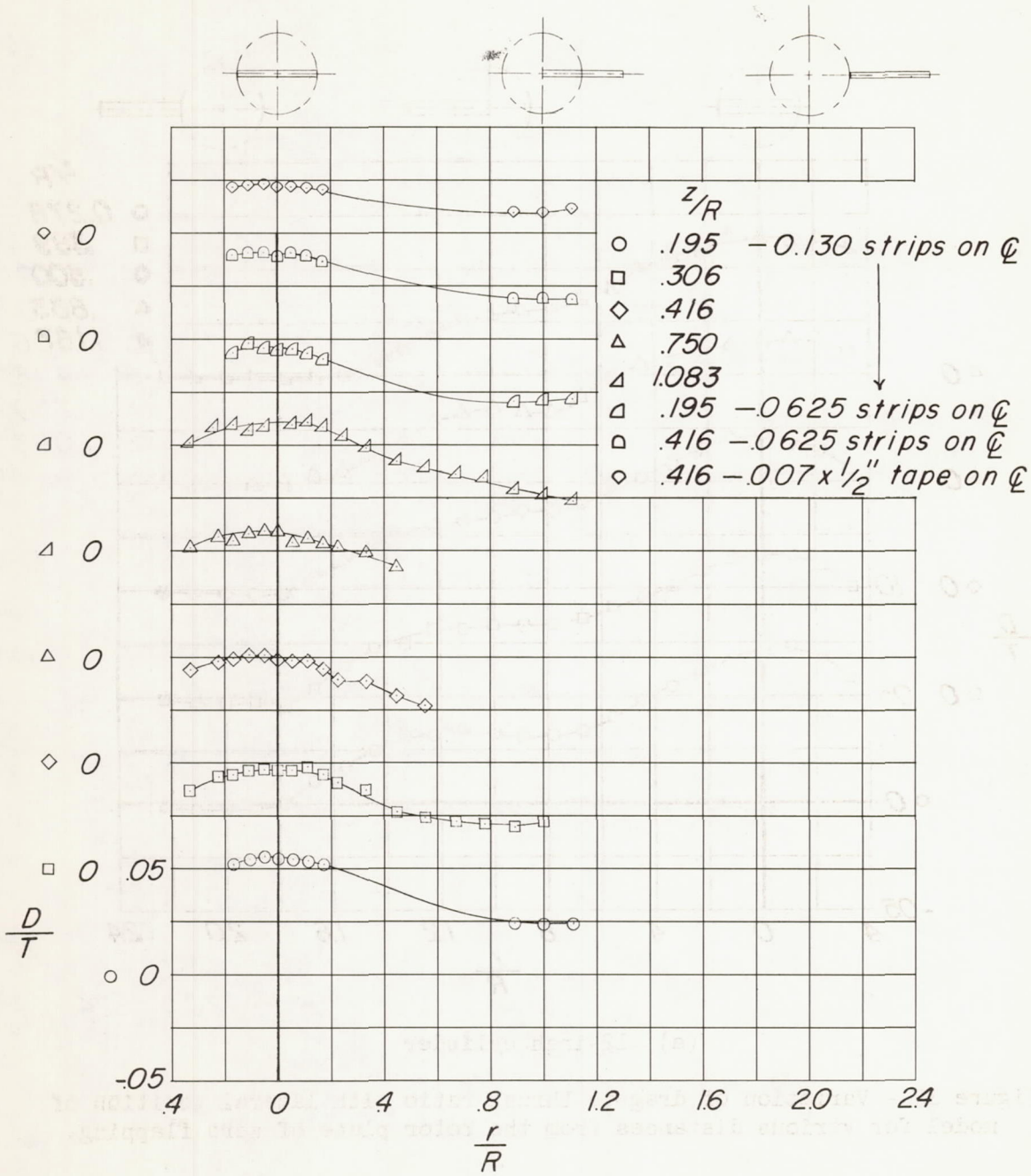

(b) 6-inch cylinder with strips.

Figure 16.- Concluded.

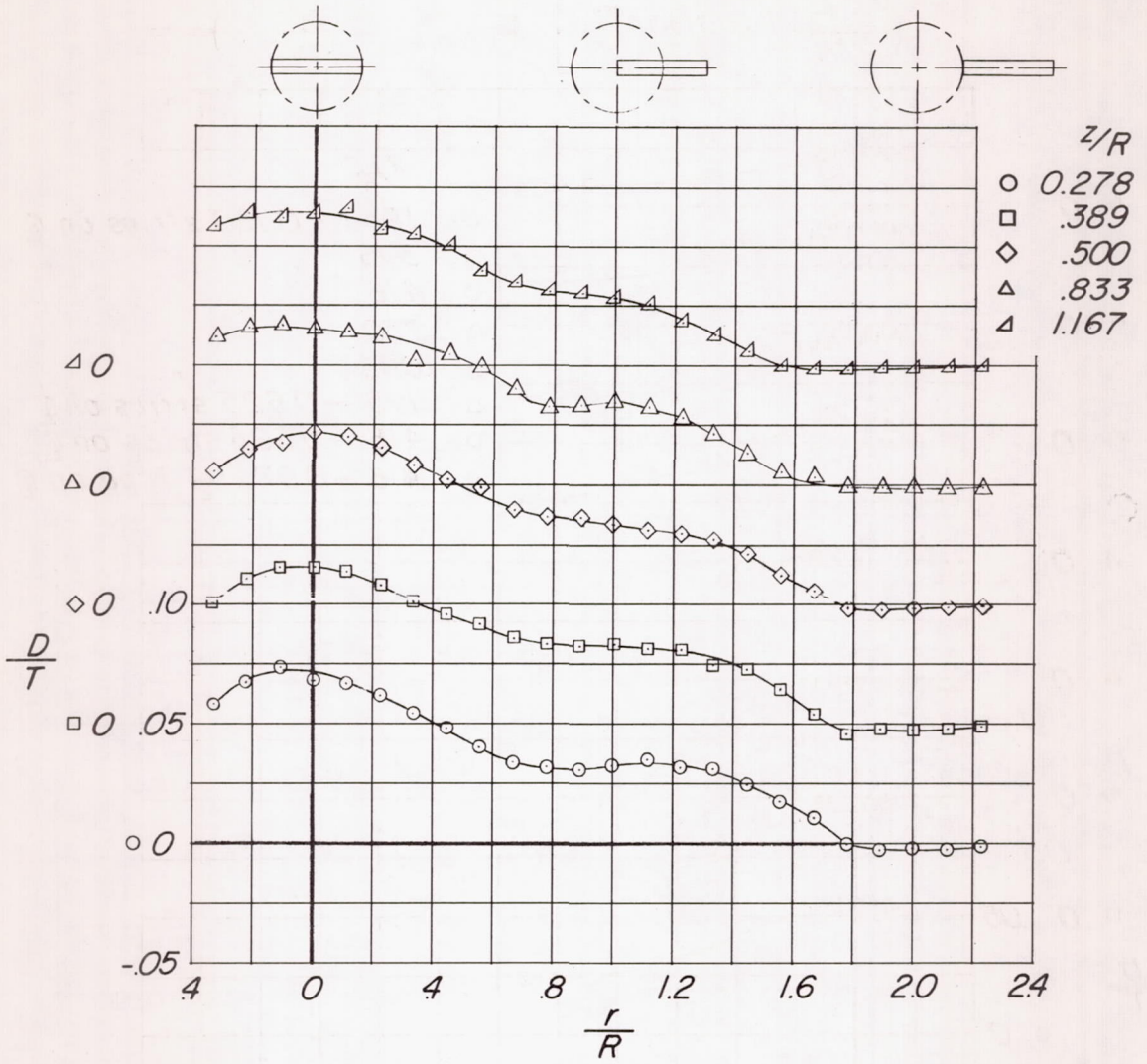

(a) 12-inch cylinder.

Figure 17.- Variation of drag-to-thrust ratio with lateral position of model for various distances from the rotor plane of zero flapping.

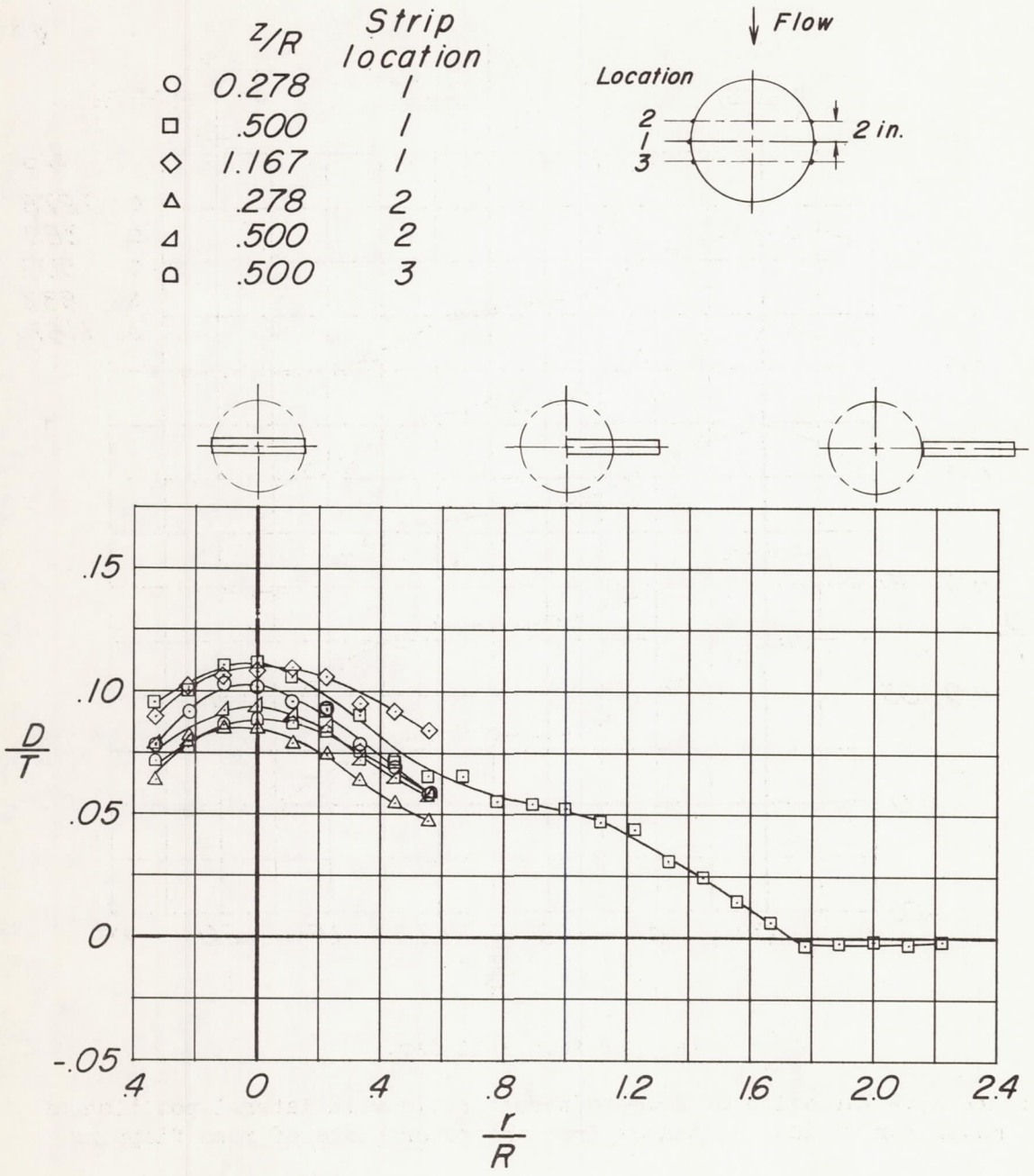

(b) 12-inch cylinder with 0.130D strips.

Figure 17.- Concluded.

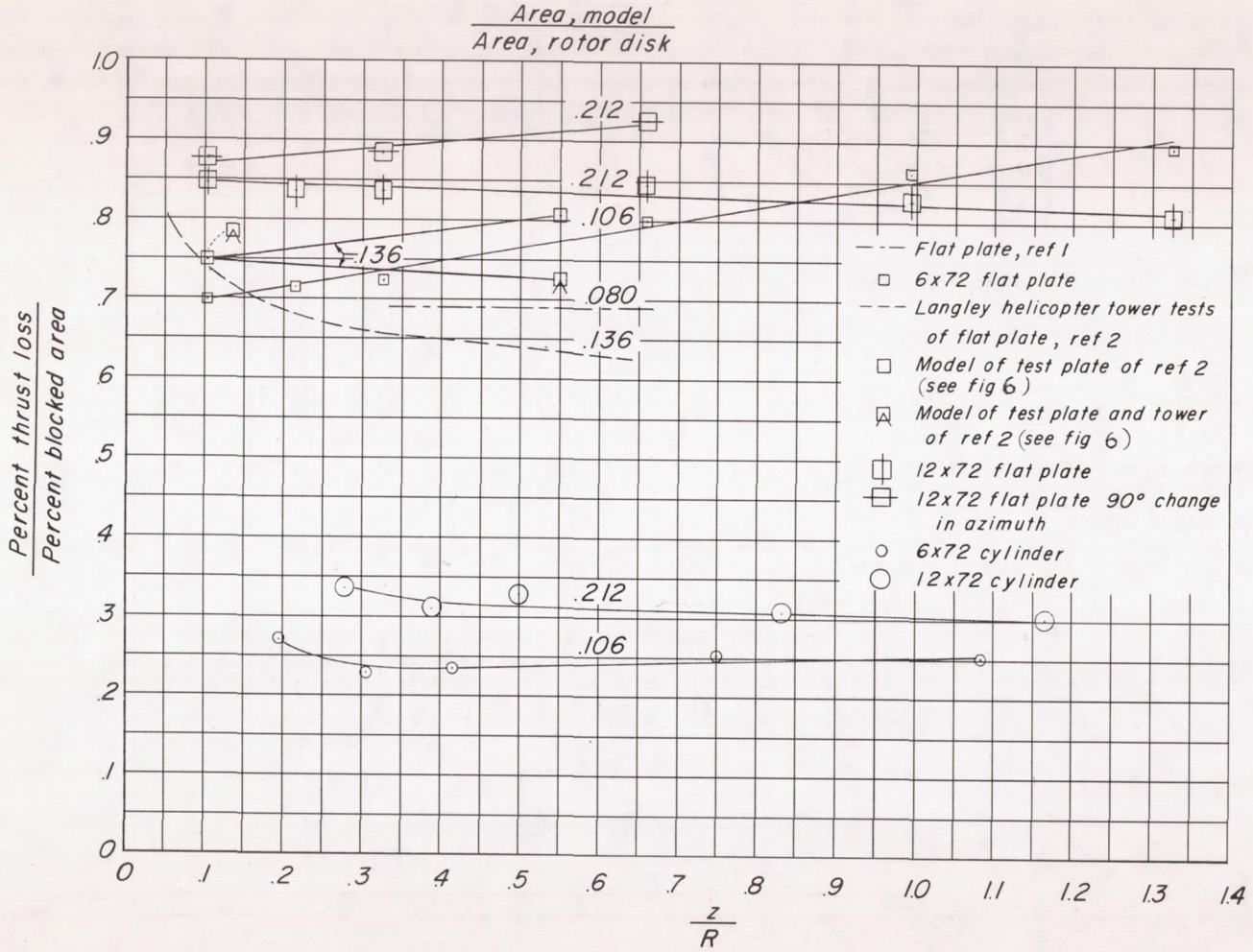

Figure 18.- Ratio of percent thrust loss due to model drag to percent blocked area of rotor disk as a function of distance from the rotor plane of zero flapping for models spanning the rotor disk.

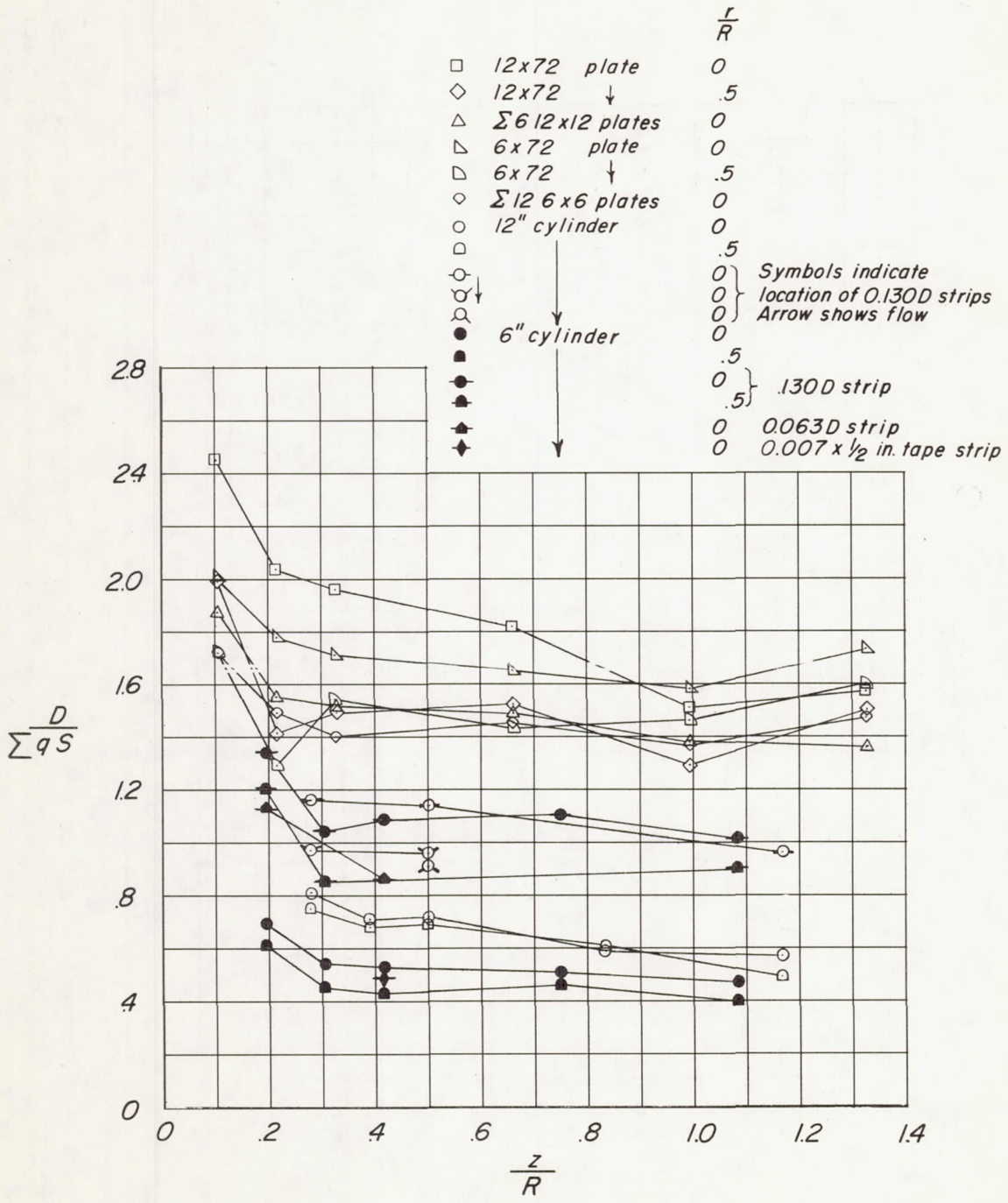

Figure 19.- Model drag coefficients as functions of distance from the rotor plane of zero flapping.